nature protocols

PROTOCOL

https://doi.org/10.1038/s41596-021-00660-9

Check for updates

Universal platform for the generation of thermostabilized GPCRs that crystallize in LCP

Jendrik Schöppe[1,2], Janosch Ehrenmann[1,3], Yann Waltenspühl[1] and Andreas Plückthun[1]✉

Structural studies of G-protein-coupled receptors (GPCRs) are often limited by difficulties in obtaining well-diffracting crystals suitable for high-resolution structure determination. During the past decade, crystallization in lipidic cubic phase (LCP) has become the most successful and widely used technique for obtaining such crystals. Despite often intense efforts, many GPCRs remain refractory to crystallization, even if receptors can be purified in sufficient amounts. To address this issue, we have developed a highly efficient screening and stabilization strategy for GPCRs, based on a fluorescence thermal stability assay readout, which seems to correlate particularly well with those GPCR constructs that remain native during incorporation into the LCP. Detailed protocols are provided for rapid and cost-efficient mutant and construct generation using sequence- and ligation-independent cloning, high-throughput magnetic bead-based protein purification from small-scale expressions in mammalian cells, the screening and optimal combination of mutations for increased receptor thermostability and the rapid identification of suitable chimeric fusion protein constructs for successful crystallization in LCP. We exemplify the method on three receptors from two different classes: the neurokinin 1 receptor, the oxytocin receptor and the parathyroid hormone 1 receptor.

Introduction

G-protein-coupled receptors (GPCRs) are a diverse family of integral membrane proteins that share a conserved membrane-embedded structure of seven transmembrane α-helices. GPCRs play a pivotal role in intercellular signalling and regulate diverse physiological processes; thus, they represent key drug targets[1,2]. As a result of enormous efforts across academia and industry, the past two decades have provided unprecedented insights into the molecular details of the structure and function of GPCRs through the determination of high-resolution structures[3–7]. At the time of writing, 93 unique receptor crystal structures have been deposited in the Protein Data Bank. However, major hurdles at all stages of the structure determination process remain, and thus obstacles to structural studies of many receptors of interest continue to hamper the field. Many GPCRs cannot be heterologously expressed in sufficient quantity and quality and do not display sufficient stability once removed from their native lipid bilayer during the purification stage[8,9]. Even if the aforementioned obstacles can be successfully overcome, the dynamic nature of GPCRs[10] and their limited hydrophilic regions available to form potential crystal contacts represent another major obstacle in obtaining protein crystals of diffraction quality.

The successful determination of GPCR structures during the past years has been made possible by the inclusion of several key technologies into the field of GPCR structural biology: (1) protein engineering approaches including the truncation of flexible termini[11], insertion of stable, hydrophilic fusion proteins[12,13], directed evolution towards increased expression levels and stability[14–17] and introduction of thermostabilizing mutations derived from exhaustive alanine (Ala) scanning[8,18,19], (2) screening of available ligands and identification of those that maximally stabilize a given receptor[20–22], or even the de novo development of tool compounds to stabilize a receptor of interest[23,24], and (3) miniaturization and automation of crystallization in lipidic cubic phase (LCP)[25–27].

However, many of these technological advances depend on and are limited by factors that are unique to every receptor of interest. The throughput and screening possibilities can be severely limited by the time and costs it takes to generate constructs, insufficient expression levels, the lack of radiolabeled ligands (e.g., for thermostabilization of GPCRs by Ala scanning using the reported

[1]Department of Biochemistry, University of Zürich, Zurich, Switzerland. [2]Present address: Novo Nordisk A/S, Måløv, Denmark. [3]Present address: leadXpro AG, PARK InnovAARE, Villigen, Switzerland. ✉e-mail: plueckthun@bioc.uzh.ch

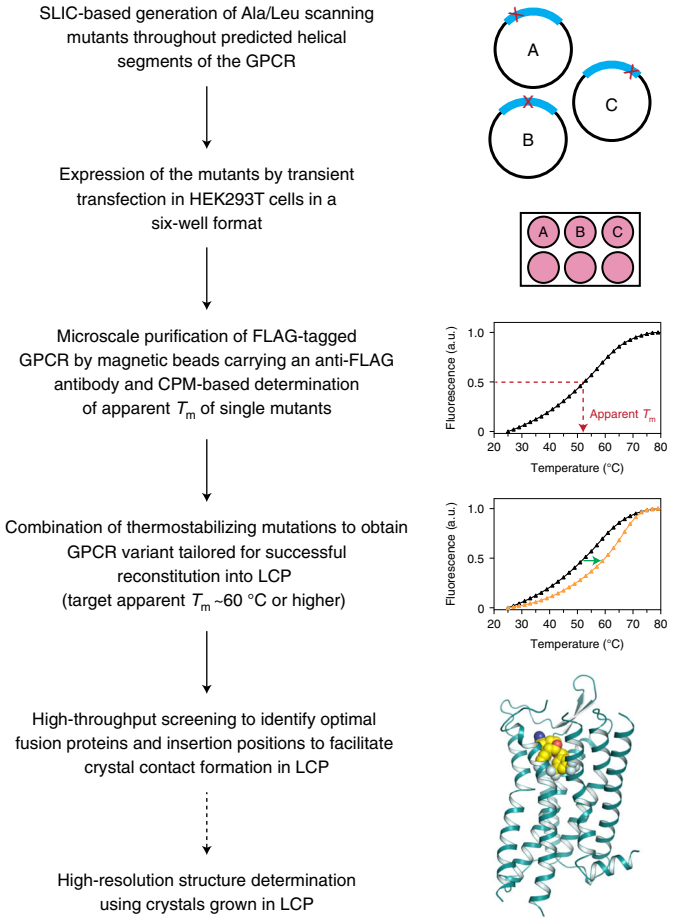

Fig. 1 | Flowchart illustrating the main steps to obtain optimally thermostabilized GPCR mutants tailored for successful crystallization in LCP. Results from the CPM-based thermostability assay were found to correlate particularly well with efficient receptor reconstitution into the monoolein bilayer and subsequent crystal formation; Therefore, these results guide the selection of single mutants, mutant combinations and fusion constructs. After the iterative microscale screening rounds in HEK293T cells, only highly promising candidates are progressed to time- and resource-intensive large-scale protein expression in insect cells and purification efforts that are necessary for structure determination.

methods[28]), absence of stabilizing ligands, or, if several of these points could be successfully addressed, failure in crystallization trials.

To overcome these complex bottlenecks in the most challenging receptors, typically strategies for improving functional expression[29] and further thermostabilization will have to be combined. We report here the development of a modular platform that allows for the rapid and cost-effective generation and screening of stabilized GPCR mutants and potential crystallization constructs. Our pipeline consists of optimized sequence- and ligation-independent cloning (SLIC), the high-throughput expression and microscale purification of GPCRs for fluorescence-based stability screening, the tailored thermostabilization of GPCRs for successful reconstitution into LCP and the accelerated identification of chimeric fusion constructs suitable to obtain high-resolution structures from crystals grown in LCP (Fig. 1). The application of the provided methodology and workflow to GPCRs of class A and B has allowed us to determine several high-resolution crystal structures of these receptors, exemplified by the neurokinin 1 receptor (NK_1R)[30], oxytocin receptor (OTR)[31] and parathyroid hormone 1 receptor (PTH1R)[32].

Development of the protocol

Thermostability of GPCRs in the CPM assay and consequences for crystallization in LCP

The fluorescence-based thermal stability assay applied in our study was initially reported in 2008 as a method to assess the thermal stability of purified, detergent-solubilized membrane proteins[33].

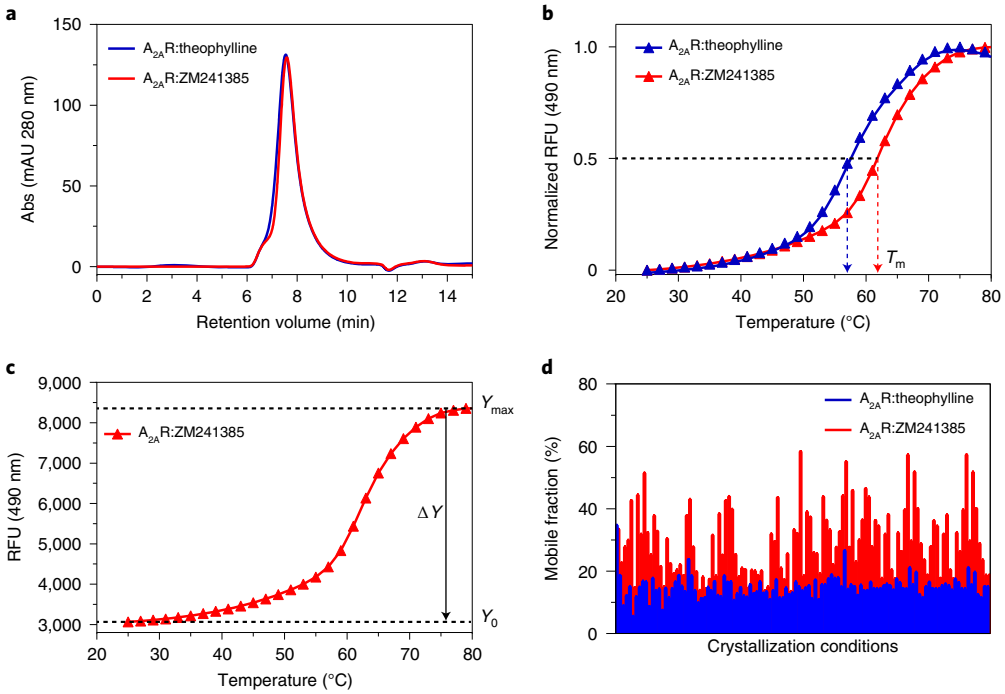

Fig. 2 | Effects of different antagonists on SEC elution profiles, the thermal stability in the CPM assay, and the mobile fraction in FRAP experiments, exemplified by theophylline- and ZM241385-bound $A_{2A}R$ ($A_{2A}R$-bRIL-ΔC, Protein Data Bank ID: 4EIY). a, Representative analytical SEC profiles of $A_{2A}R$, purified from the same batch of *Sf*9 insect cell membranes in 0.05%/0.01% (wt/vol) DDM/CHS, in the presence of either theophylline or ZM241385. Analytical SEC was performed on an Agilent 1100 HPLC system using a Sepax Nanofilm SEC-250 column. **b**, Representative CPM-based thermostability measurements of 1.0 μg of purified $A_{2A}R$ in 20 μl of buffer from the same purifications as in **a**, measured in the presence of theophylline or ZM241385. Samples were equilibrated for 5 min at 25 °C followed by a 2 °C/min thermal ramp from 25 °C to 95 °C. The apparent T_m of $A_{2A}R$ depends on the bound antagonist; $A_{2A}R$:theophylline, apparent T_m 57.6 °C (indicated by blue arrow); $A_{2A}R$:ZM241385, apparent T_m 61.8 °C (indicated by red arrow). Note that the *y*-axis is min–max normalized. **c**, Raw data plot of thermal stability measurement of $A_{2A}R$:ZM241385 with CPM. Y_0 corresponds to the CPM fluorescence baseline and Y_{max} to the fluorescence signal at the plateau, indicated as dashed black lines. $\Delta Y = Y_{max} - Y_0$ represents the maximal attainable CPM fluorescence amplitude in the given measurement and is indicated as a black arrow. This measure reflects the amount of protein that can interact with CPM, and thus translates to expression and purification yield. All thermostability measurements were performed on an Agilent Mx3005p qPCR thermal cycler. **d**, Representative LCP-FRAP experiments for $A_{2A}R$:ZM241385 and $A_{2A}R$:theophylline. Bar graph representation of the mobile fraction of $A_{2A}R$:ZM241385 (red bars) and $A_{2A}R$:theophylline (blue bars) in 96 different screening conditions. $A_{2A}R$:ZM241385 displays an overall substantially higher mobile fraction than $A_{2A}R$:theophylline in all of the tested conditions. Purified receptor was fluorescently labeled using Cy3 NHS ester, reconstituted into LCP, overlaid with precipitant solution and equilibrated for 12 h. LCP-FRAP was measured using a Formulatrix FRAP Benchtop device. RFU, relative fluorescence units.

In short, the thiol-reactive fluorophore *N*-[4-(7-diethylamino-4-methyl-3-coumarinyl)phenyl]maleimide (CPM)[34] was used with the intention to probe the accessibility of native cysteine residues preferably located in helix–helix interfaces. When the protein unfolds in response to a temperature gradient, these cysteine residues would become accessible to covalent modification, whereupon intrinsic CPM fluorescence increases and a detectable signal is generated. Protein stability can thus be assessed by the apparent melting temperature in a thermal unfolding experiment. It was later shown, however, that the assay also works in the absence of any cysteines[35], suggesting that the fluorescence increase is at least partly caused by binding of the fluorophore to hydrophobic patches or crevices that become exposed upon partial protein unfolding.

While establishing the purification and crystallization in LCP of the adenosine A_{2A} receptor ($A_{2A}R$) as a model system for other GPCRs, we recognized that, although analytical size-exclusion chromatography (aSEC) profiles and the overall yield of $A_{2A}R$ purified in the presence of two different antagonists (theophylline and ZM241385, a synthetic adenosine analog) were identical (Fig. 2a), only ZM241385-bound $A_{2A}R$ yielded crystals in the LCP. Subjecting the purified receptor samples to the CPM assay revealed that ZM241385-bound $A_{2A}R$ displayed a substantially higher apparent melting temperature (T_m) of 61.8 °C than the theophylline-bound $A_{2A}R$ (57.6 °C) (Fig. 2b).

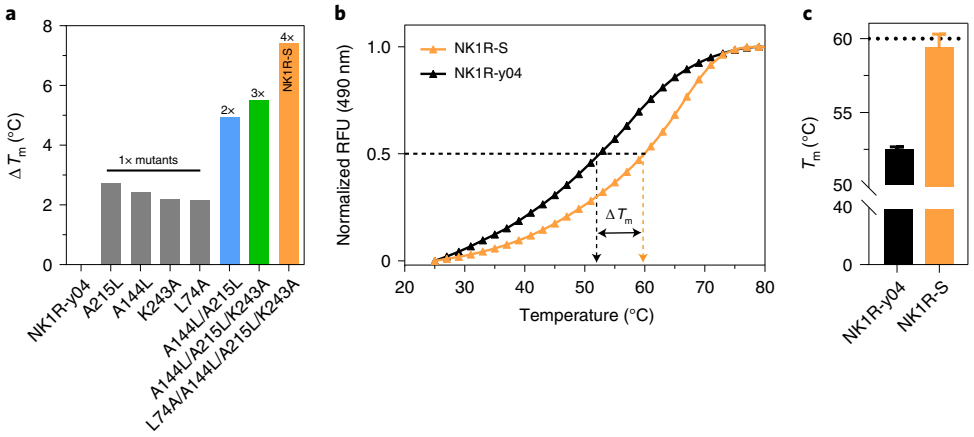

Fig. 3 | CPM-based thermostabilization of NK_1R-y04 in an antagonist-bound conformation. a, ΔT_m derived from the apparent CPM melting temperature of the four single-point mutants (gray bars) and the double (blue bar), triple (green bar) and the quadruple mutant NK_1R-S (orange bar) as compared with the receptor variant NK_1R-y04. **b**, Comparison of the CPM-derived thermostability of NK_1R-y04 (black curve) and the quadruple mutant NK_1R-S (orange curve). The apparent T_m is indicated by a dashed black and orange arrow, respectively. **c**, Average apparent T_m of NK_1R-y04 (52.4 °C, $n = 12$ independent expressions, purifications and measurements) and NK_1R-S (59.4 °C, $n = 8$ independent expressions, purifications and measurements) with standard deviations represented by error bars. NK_1R-y04 and all mutants were expressed and purified by anti-FLAG antibody-containing magnetic beads as described in the Procedure. During solubilization and purification of the receptor, the small-molecule antagonist CP-99,994 was added to all buffers at saturating concentrations. All thermostability measurements were performed on an Agilent Mx3005p qPCR thermal cycler.

Importantly, the observed difference in apparent melting temperature (ΔT_m) also correlated with differences in the measured mobility of $A_{2A}R$ in fluorescence recovery after photobleaching (FRAP) experiments performed with fluorescently labeled receptor reconstituted into LCP (LCP-FRAP)[36]: while ZM241385-bound $A_{2A}R$ displayed mobility representing diffusion in the LCP matrix (a prerequisite for crystal formation), in multiple conditions, theophylline-bound $A_{2A}R$ showed no diffusion in any of the tested conditions (Fig. 2d). We hypothesized that the theophylline-bound $A_{2A}R$ may have become aggregated in the LCP matrix owing to insufficient stability.

Furthermore, the analysis of published, unique GPCR crystal structures for which a CPM-derived T_m has been reported[12,22–24,37–62] indicates that a large majority (>90%) of GPCRs that were successfully crystallized in LCP displayed a $T_m \geq 60$ °C (similar to ZM241385-bound $A_{2A}R$), and the remaining receptors exhibit at least a $T_m > 58$ °C. Taken together, these data suggested to us that a CPM-derived T_m of ideally ≥60 °C might be an indicative parameter to predict whether a given receptor will successfully reconstitute into the lipid bilayer during formation of the LCP (a critical prerequisite for obtaining protein crystals[63]).

Our research on yeast-evolved variants of the human NK_1R (variant NK_1R-y04) and PTH1R (variant PT-y03)[17] showed that, despite increased expression and purification yields of these mutants, their CPM-derived apparent melting temperatures were still in the low 50 °C range (Fig. 3). Consequently, and regardless of great efforts in crystallization construct design, purification optimization and crystallization trials in LCP, we never observed crystals or mobility in LCP-FRAP experiments of theses receptors.

We therefore hypothesized that increasing the CPM-T_m of these receptors to ≥60 °C would yield variants that are specifically thermostabilized for reconstitution into LCP and ultimately would yield structures of our target proteins. Consequently, we posited that measuring the T_m by a CPM-based assay would guide us to such variants. To achieve this targeted stabilization, we devised a comprehensive high-throughput platform from construct generation to microscale expression and purification, which harnesses the fluorescence-based CPM assay as a particularly relevant readout and selection criterion.

Sequence- and ligation-independent cloning

For high-level protein expression of GPCRs, we constructed the expression vector pcDNA5_SLIC (Fig. 4a) and devised a modular and flexible SLIC-based mutant and construct generation toolbox (Fig. 4b).

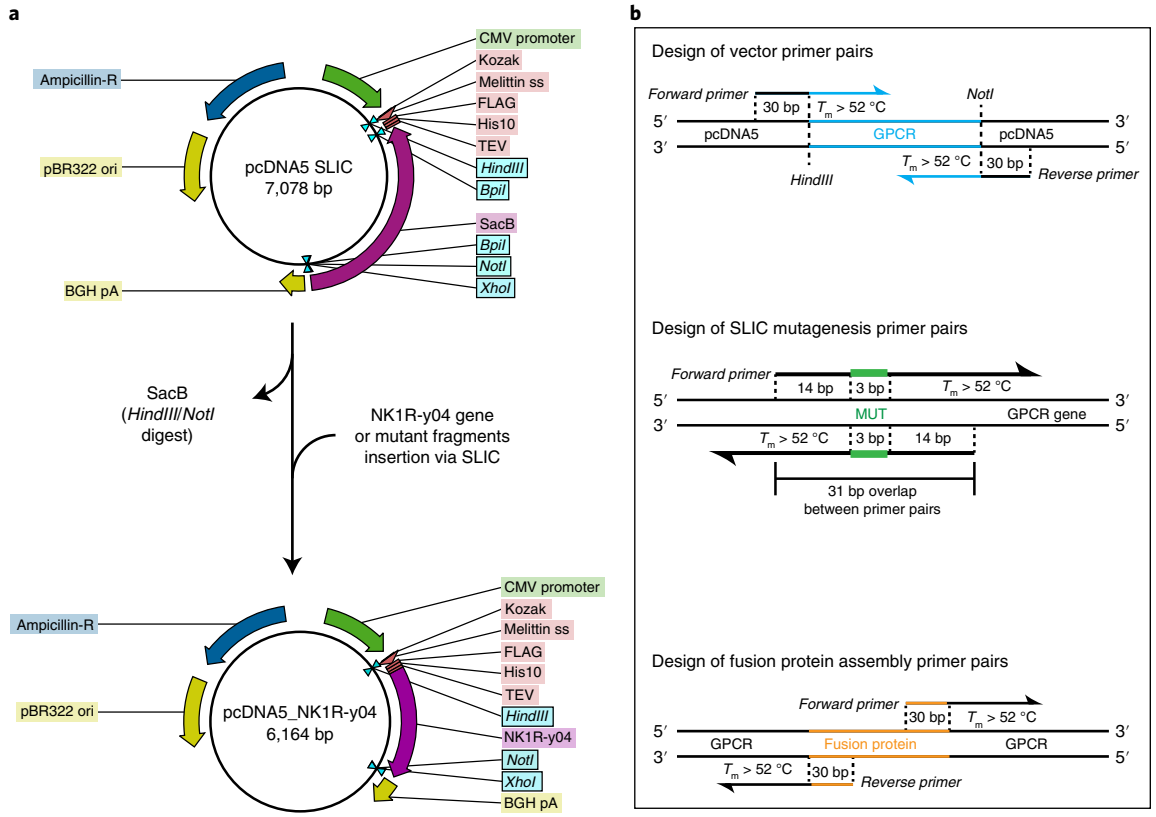

Fig. 4 | Modular SLIC-based cloning and construct generation toolbox. a, For the generation of the high-copy expression vector pcDNA5_NK$_1$R-y04 (bottom), the *sacB* counter-selection cassette is excised from the cloning vector pcDNA5_SLIC using the restriction enzymes HindIII and NotI and subsequently replaced by the NK$_1$R-y04 gene using SLIC. Specifications: CMV promoter, Kozak consensus sequence (Kozak), melittin signal sequence (Melittin ss), FLAG epitope (FLAG), His$_{10}$-tag (His10), TEV protease cleavage site (TEV), levansucrase-encoding counter selection cassette (SacB), bovine growth hormone polyadenylation signal (BGH pA), ampicillin resistance gene (Ampicillin-R), pBR322 origin of replication (pBR322 ori). **b**, Illustration of the design of specific primer pairs used in the PCR-based insert fragment generation for SLIC. Vector primers (top) anneal on the GPCR insert (highlighted in blue) and carry overhangs homologous to the target vector. SLIC mutagenesis primers (middle) introduce a specific mutation (highlighted in green) in the overlapping homologous region of an N- and a C-terminal GPCR fragment. Fusion protein assembly primers (bottom) anneal on the GPCR and carry overhangs homologous to the fusion protein (highlighted in orange).

SLIC is a highly versatile cloning method[64] (Fig. 4), based on in vitro homologous recombination and in vivo single-strand annealing repair after transformation of *Escherichia coli* cells with the annealed DNA fragments[65]. The method was conceived to circumvent the sequence restrictions of traditional cloning methods such as restriction-enzyme-based cloning[66]. Thus, SLIC offers the advantage that any vector can be used and the introduction of additional base pairs in the insert gene by restriction enzyme recognition sites can be avoided.

Briefly, SLIC consists of five steps:

(i) initial linearization of the vector backbone by restriction enzyme digest
(ii) generation of insert fragments with homologous overhangs by PCR
(iii) incubation of both vector and insert fragments with T4 DNA polymerase in the absence of dNTPs to generate single-stranded overhangs via the T4 DNA polymerase's 3′-5′ exonuclease activity
(iv) in vitro annealing of the generated vector and insert fragments
(v) transformation of *E. coli* cells with the annealed fragments

Compared with traditional cloning methods, SLIC further allows the efficient assembly of multiple DNA fragments in a single reaction with high fidelity, thus greatly facilitating the generation of multifusion proteins. Because of the high fidelity and great versatility of SLIC, we established an optimized protocol for our construct generation workflow and furthermore adapted the method as an attractive alternative to existing site-directed mutagenesis protocols.

The SLIC-based mutagenesis approach described here has two major advantages over QuikChange mutagenesis (Agilent) or equivalent protocols that are typically used for site-directed mutagenesis: (i) the vector does not undergo PCR amplification, therefore avoiding the need for recloning of the

mutated gene in a second step to ensure plasmid integrity; (ii) the insert fragment generation by PCR is compatible with very low template DNA concentrations, making an additional step of enzymatic template digestion after PCR unnecessary.

Although the protocol provided here describes the introduction of single-point mutations in the coding sequence of the human NK_1R, it is universally applicable to all SLIC-based cloning projects. The vector carries a *sacB* gene, which can be counter-selected in the presence of high sucrose concentrations[67], thereby ensuring high-efficiency insertion of the gene of interest (GOI). Briefly, periplasmic SacB converts sucrose to levan, which is toxic to *E. coli*, and thus replacement of *sacB* allows colonies to grow.

For users unfamiliar with the SLIC procedure, it is highly recommended to start with a smaller subset of mutants (e.g., two to three) to get familiar with the protocol.

Small-scale high-throughput expression of GPCRs

The most widely used expression system for the production of GPCRs for structural studies are *Spodoptera frugiperda* (*Sf*9) insect cells[68]. However, the need for baculovirus generation and amplification severely limits the throughput and increases the lead times required from initial cloning steps to protein production (~4 weeks). Thus, expression of GPCRs in *Sf*9 insect cells represents a major bottleneck for any screening approach. To allow the anticipated high throughput needed to perform the screening of up to 400 different receptor mutants or constructs, we established receptor expression by transient transfection of HEK293T cells. In this way, the receptors can be expressed at reasonably high levels, so that expression of multiple mutants can be performed on an unprecedented small scale (1–2 million HEK293T cells) in parallel. Furthermore, the expressed receptor variants can readily be solubilized by mild detergents (e.g., *n*-dodecyl-β-D-maltopyranoside/cholesteryl hemisuccinate (DDM/CHS)) from the plasma membrane of HEK293T cells without mechanical cell disruption. After the receptor of interest (e.g., NK_1R-y04, that had previously been evolved in yeast[17]) is cloned into pcDNA5_SLIC and HEK293T cells are transiently transfected with the plasmid, NK_1R-y04 (in this example) is produced in a form that carries an N-terminal melittin signal sequence, followed by a FLAG epitope, a His_{10} tag and a tobacco etch virus (TEV) protease cleavage site in front of the actual receptor open reading frame. This expression format allows freedom with regard to the purification method and has been shown to work for a large variety of different GPCRs.

Microscale purification of GPCRs

The purification of GPCRs remains another major bottleneck, so far hindering the necessary throughput for simultaneously screening and characterizing many different possible receptor mutants or constructs. Independent of the chosen expression system, the receptor purification procedure usually involves chromatography-based separation, during which the detergent-solubilized protein is isolated and purified for subsequent downstream applications. These labor-intensive and time-consuming steps require relatively large amounts of starting material and only allow the parallel purification of a small number of different protein samples; additionally, a 2 d minimum time frame for any purification is required in our experience.

To address these issues, we have developed a method that drastically increases the achievable throughput, while reducing the required time for purification. In the manual format described in the Procedure, the method allows for the parallel purification of up to 30 receptors (or mutants) within <8 h with final protein yields of ~0.5–2 μg.

This unprecedented throughput for membrane protein purification is achieved by employing magnetic beads[69] functionalized with the anti-FLAG M2 monoclonal antibody[70] for the isolation, separation and purification of FLAG epitope-fused receptor constructs. After whole-cell solubilization, the sample is incubated with the magnetic beads, and thus FLAG-tagged receptor is captured from the suspension with high specificity and affinity.

Subsequent washing steps to achieve high purity of the sample are performed by collecting the beads with a magnetic separator, allowing for rapid separation from the solubilization and wash buffer solutions. Mild elution of the receptor from the antibody is achieved in very low volumes by competition with an excess of free 3× FLAG peptide, resulting in sufficiently high concentrations of receptor. The microscale purification results in protein samples of high purity, comparable to chromatography-based large-scale purified receptor as evidenced by the identical CPM-derived melting curves obtained for NK_1R-S_1207 (Fig. 5c,d). To date, we have successfully employed the microscale purification method for several different wild-type and yeast-evolved GPCRs.

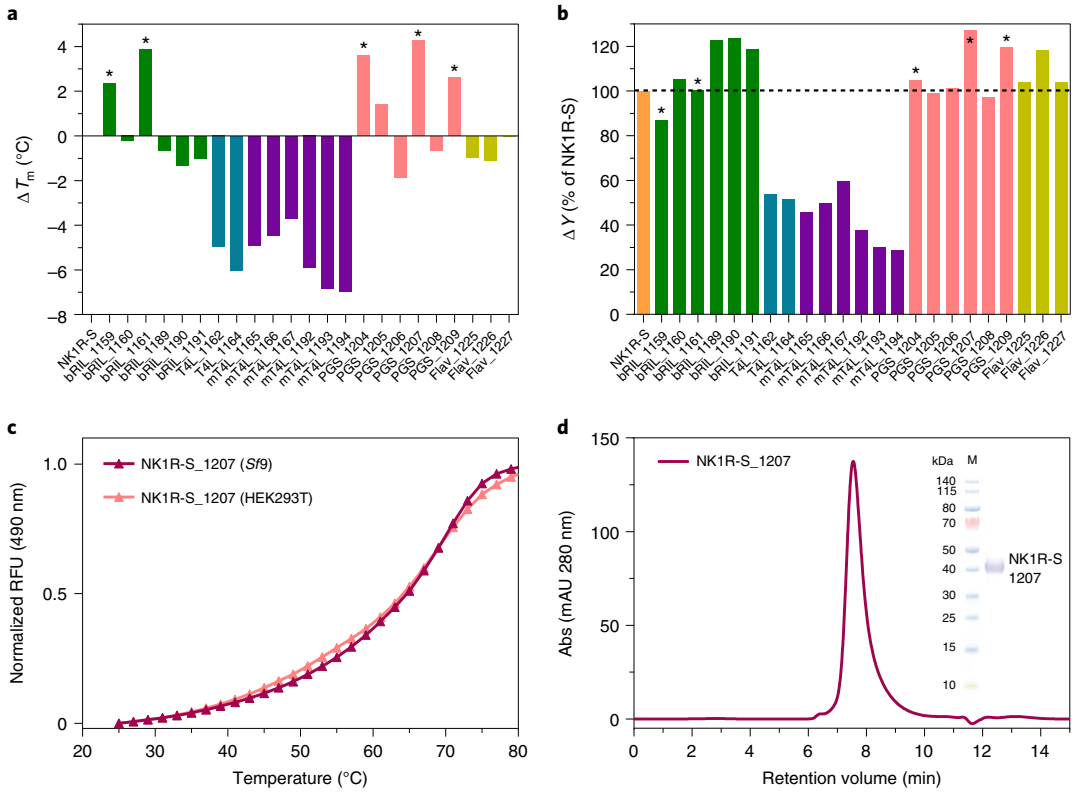

Fig. 5 | CPM-based screening of fusion proteins and insertion positions to replace the ICL3 of NK_1R-S for crystallization in LCP. a, ΔT_m of tested chimeric fusion constructs compared with the thermostabilized, nonfused mutant NK_1R-S. **b**, Difference in expression and purification yield of the same fusion constructs compared with NK_1R-S from the signal amplitude in the CPM assay. The expression and purification yield, expressed as ΔY (Fig. 2c), of each construct is compared with that of NK_1R-S (set to 100%, dashed line). Fusion constructs marked with an asterisk, showing both favorable ΔT_m and ΔY, were selected for large-scale expression in *Sf*9 insect cells and subsequent crystallization trials in LCP. **c**, Comparison of CPM-derived thermostability of construct NK_1R-S_1207 purified from HEK293T cells and from large-scale expression and purification from *Sf*9 insect cells. The great similarity is apparent. The purification from HEK293T cells was performed as described in the Procedure. Large-scale purification from *Sf*9 insect cells was performed as previously described[30]. **d**, Representative aSEC profile and sodium dodecyl sulfate–polyacrylamide gel electrophoresis gel of construct NK_1R-S_1207 bound to CP-99,994 purified from *Sf*9 insect cells. All thermostability measurements shown were performed in the presence of 50 μM CP-99,994 on an Agilent Mx3005p qPCR thermal cycler.

CPM-based thermostabilization: antagonist-bound NK_1R-y04

The yeast-evolved human NK_1R variant NK_1R-y04 (ref. [17]) was initially selected to test our hypothesis regarding the possibility to use the CPM assay as a measure for the tailored thermostabilization of GPCRs. For this purpose, we generated 178 single-point mutants of NK_1R-y04 using SLIC-based mutagenesis and construct generation approach described below. To limit the number of mutants, and hypothesizing from previous directed evolution data on different receptors that most of the stability of the receptor is conferred by interactions within the heptahelical transmembrane bundle, we focused mutagenesis on positions predicted to be located in transmembrane α-helices and changed each amino acid to alanine (Ala) (or leucine (Leu) if the position already was an Ala).

Mutation to Ala is widely performed in screening approaches to determine the contribution of a specific residue to the stability (or function) of a protein since Ala is chemically inert, will not introduce a clashing side chain, and has a high helical propensity. With emphasis on the thermostabilization through Ala screening of membrane proteins that are helical bundles, the underlying assumption is that exchanging a bulky side chain with an Ala might enable closer interaction between two helices, thereby increasing stability. On the other hand, positions within the helix that are already occupied with Ala might profit from exchange to Leu. With its hydrophobic γ-branched side chain, it is very compatible with helix packing, Leu might fill in a hydrophobic pocket in the interface to an adjacent helix, thereby strengthening the interaction and thermostability.

Thus, at each mutated position, the contribution of the wild-type amino acid side chain to protein stability is probed by removing all atoms past the β-carbon, without interfering with secondary structure preferences[71,72]. Each mutant was expressed, purified in the presence of the small molecule

antagonist CP-99,994, and subjected to the CPM assay to determine its T_m. For each batch of measurements, NK_1R-y04 was included as a control to allow determination of the relative ΔT_m of each mutant. From this initial round of screening, we found that ~10% of the mutations were thermostabilizing with an increase of relative ΔT_m 2–3 °C in the CPM assay (a subset is shown as gray bars in Fig. 3a). Therefore, to reach a T_m of ~60 °C, it was necessary to combine several thermostabilizing mutations.

Care should be taken to analyze each beneficial single-point mutation identified during initial screening with regard to its influence on purification yield as well as its location in the possible tertiary structure (i.e., helical interfaces). For example, during stabilization of NK1R-y04, identified mutations were mapped onto the solved structure of the related orexin 2 receptor[73]. Using this strategy, beneficial mutations that are directly opposing each other in a helix–helix interface can be identified. Subsequently, only one of both should be used for further combinatorial studies to avoid steric interference, as the beneficial effect may have been limited to either mutation being in the wt context.

The results of the initial screening might vary widely in number of mutants and detected ΔT_m values. Therefore, to limit the number of combinatorial constructs but ensure proper screening and success in thermostabilization, a cutoff value based on relative ΔT_m should be chosen (here ≥2 °C, typically rendering ~10% of the mutants above the cutoff).

However, for selecting those mutants to progress to the first round of combining mutations (termed '2× mutants'), we did not solely rely on the measured ΔT_m value, but also considered the signal amplitude of the assay, ΔY, as an indicator of functional expression and purification yield (Fig. 2c). As previously described[74], the most rapid method for effectively combining stabilizing mutations is to use the most stable mutant as a basis and then to add each of the other identified stabilizing mutations to it, assuming a certain degree of additivity of the mutations. For this purpose, we created a series of double mutants using the already available SLIC mutagenesis primers together with the DNA of the most stable mutant as a PCR template.

The ΔT_m values were determined from the expressed and purified double mutants, with the most promising double mutant displaying a T_m increase of 4.9 °C, which is almost additive of the single mutants (Fig. 3a, blue bar), when compared with NK_1R-y04. This double mutant then served as the basis for the generation of triple mutants. Yet, single mutations that did not show a thermostabilizing effect in the double mutant experiments were not further progressed, because they might be mutually exclusive, as certain mutations might be stabilizing slightly different receptor conformations. Since we had initially hypothesized and thus defined a 'target' T_m of ~60 °C for successful reconstitution into LCP, we proceeded to construct and screen a set of quadruple mutants to achieve this goal. The most stable quadruple mutant we were able to identify (termed NK_1R-S) was 7 °C more stable in the CPM assay than the initial mutant NK_1R-y04, and showed a CPM-derived T_m of 59.4 °C (Fig. 3a–c).

CPM-based screening of chimeric fusion protein constructs for crystallization in LCP

The use of stable, hydrophilic fusion protein partners to create crystal contacts has been pivotal for almost all high-resolution GPCR structures obtained from crystals grown in LCP[4]. Originally intended to promote crystal contacts in the water channels of the LCP, it was soon appreciated that optimally inserted fusion proteins can enhance receptor stability further[13], while poorly designed fusion constructs would do the opposite[13,73]. However, the increasing number of possible fusion partners as well as the empirical determination of suitable fusion insertion positions remains a difficult optimization problem. Therefore, we have adapted the CPM-based high-throughput screening methodology also to allow the assessment of (i) suitable fusion proteins for a given receptor and (ii) optimal fusion protein insertion positions, especially as replacement of intracellular loops.

For GPCRs, the most successful approach has been the introduction of fusion partners between the C-terminal end of helix 5 and the N-terminus of helix 6 to replace the third intracellular loop (ICL3), which is highly variable in length and often found to be flexible[75,76]. While in the early years of GPCR structure determination, studies primarily relied on T4 lysozyme (T4L) as a fusion protein, it was discovered that many GPCRs were not compatible with T4L insertion as evidenced by deleterious effects on expression or stability of chimeric constructs[13]. Thus, several alternative fusion partners such as apocytochrome b_{562}RIL (bRIL), flavodoxin (Flav), mini T4 lysozyme (mT4L), rubredoxin and the catalytic domain of *Pyrococcus abyssi* glycogen synthase (PGS)[77] were identified and subsequently successfully employed in structural studies of various receptors[13,73,78].

In the absence of structural data of a receptor, the positioning of the fusion protein between the C-terminus of helix 5 and the N-terminus of helix 6 has to be determined empirically. Consequently, to identify a successful chimeric crystallization construct of a given receptor, usually many constructs with different receptor junction interfaces and various fusion domains have to be cloned, expressed and screened in crystallization trials, which is extremely time consuming and costly.

Assuming that nonoptimal junction positioning or fusion protein incompatibility with the receptor would manifest itself as a decrease in apparent T_m due to strain or distortion of the receptor helical core and that it might also result in decreased expression levels, we sought to employ our CPM-based screening platform also for the rapid generation and prescreening of chimeric crystallization constructs. We thus generated a panel of 23 potential crystallization constructs based on the thermostabilized receptor mutant NK_1R-S, using five different fusion proteins (bRIL, T4L, mT4L, PGS, Flav) at various insertion positions to replace ICL3 via the modular SLIC-based cloning methodology (Fig. 3b). After transient expression and microscale purification, we assessed each construct with regard to its T_m and signal amplitude ΔY in the CPM assay (Fig. 5a,b). The CPM-based screening resulted in the identification of several fusion positions of bRIL and PGS that resulted in a >2 °C increase in T_m together with retained or even slightly increased ΔY. These results suggested to us that these combinations of NK_1R-S, fusion protein and junction position can be considered as favorable, thus presenting attractive leads for initial crystallization trials. Furthermore, the obtained screening results clearly indicated that neither T4L nor mT4L were compatible at any tested fusion position, as evidenced by a marked decrease in the determined T_m and ΔY of all constructs carrying these insertions.

Based on the rapidly obtained prescreening results, we advanced the five top-performing fusion constructs (marked with an X in Fig. 5a,b) to large-scale expression in *Sf*9 insect cells for crystallization trials in LCP.

Expression in insect cells relies on the infection of the cells with recombinant baculovirus that carries the DNA for the GOI. Generation and amplification of baculovirus typically takes ~3–4 weeks and involves many laborious steps. However, baculovirus can then be prepared in large amounts and subsequently only needs to be added to the cells for highly efficient liter-scale expression cultures without the need for costly transfection reagents. Therefore, it is a cost-effective method to prepare milligram amounts of recombinant protein once a suitable construct has been identified. While large-scale expression in HEK is relatively quick, since the cells only need to be transfected, it is extremely expensive due to high consumption of costly reagents.

The PGS-fusion construct NK_1R-S_1207 bound to CP-99,994 could be readily purified by immobilized metal ion affinity chromatography, and showed a single, monomeric peak on aSEC (Fig. 5d) and equal thermostability in the CPM assay when compared with the same construct purified on a microscale from HEK293T cells (Fig. 5c).

Application of CPM-based thermostabilized and screened GPCRs

In agreement with our initial hypothesis that the CPM-based thermostabilization of a GPCR should result in a mutant suitable for reconstitution into LCP, NK_1R-S_1207 readily crystallized in LCP in a multitude of initially tested crystallization conditions. As a result, the receptor construct NK_1R-S_1207, engineered through CPM-based thermostabilization and fusion screening, allowed the determination of a high-resolution crystal structure of the human NK_1R in complex with the small-molecule antagonist CP-99,994 (ref. [30]). Remarkably, purification and crystallization trials of NK_1R-S_1207 in complex with further developed and clinically used NK_1R antagonists were also successful and resulted in two additional high-resolution crystal structures[30]. These results are intriguing since they suggest that, although the CPM-based thermostabilization and screening was performed with a particular ligand (CP-99,994), the resulting stabilized mutant of the receptor still allows the binding and co-crystallization with different ligands, thus allowing the determination of several co-structures of one receptor from one optimally stabilized mutant. In the search for new drugs targeting GPCRs, such an optimized receptor variant thus represents a valuable and versatile tool for structure-based drug design campaigns.

Most importantly, we were able to transfer the developed methodology to other GPCRs, such as the OTR[31], a receptor with very low expression yields, and the PTH1R, which belongs to the class B family of GPCRs[32]. In both cases the CPM-based thermostabilization and rapid screening of fusion protein constructs allowed us to solve the first crystal structure of OTR in complex with the

small-molecule antagonist retosiban at 3.2 Å resolution, and that of PTH1R in complex with a 34 amino acid peptide agonist at 2.5 Å resolution[32].

Limitations

Since the method presented here is based on the measurement of a change in fluorescence of the CPM dye as a result of the dye being exposed to a changing chemical environment (i.e., exposure of previously buried cysteine residues due to protein unfolding upon temperature increase and/or increased binding to a hydrophobic patch or crevice), ambiguous melting curves represent an important limitation. These might be caused by (i) buffer components interacting with the CPM dye, (ii) intrinsic fluorescence of buffer components (e.g., ligands), (iii) low protein quality or (iv) low protein quantity. To detect and account for such effects, appropriate controls should always be included (see Troubleshooting section for more information). The effect of additional buffer components always needs to be assessed in preliminary experiments. Due to the maleimide group of the dye, the assay is not compatible with reducing agents. To prevent the formation of intermolecular disulfide bonds, alkylating agents such as iodoacetamide should be used prior to solubilization. For each receptor ligand the concentration has to be optimized beforehand, in particular when peptide ligands are used, to avoid an elevated background signal. Ligands with inherent fluorescence spectra overlapping with that of the CPM dye have to be excluded as they cannot be used at saturating conditions.

Since the CPM-based screening relies on the detection of the thermal partial unfolding of purified receptor, contaminated, nonhomogeneous protein preparations may result in ambiguous melting curves. However, due to the fast and efficient nature of the cloning and screening methods provided herein, expression conditions (length, temperature, additives, transfection conditions), initial expression constructs (signal sequences, truncations, generic mutations) and purification conditions can be screened and optimized in rapid cycles with substantially reduced resources and improved timelines compared with other methods.

Furthermore, the choice of detergent for protein solubilization may influence the success of the described stabilization method. This protocol was developed for proteins solubilized in DDM/CHS, the detergent most widely used for structure determination of eukaryotic membrane proteins from crystals grown in LCP. While other detergents may also be compatible with the method, these detergents have to be validated beforehand with regard to yielding interpretable melting curves. Importantly, the apparent stability of receptors purified in different detergents may vary, and thus the target T_m of 60 °C formulated for proteins solubilized in DDM/CHS may be different in such detergents.

Finally, while we found that a T_m > 60 °C is indicative of sufficient receptor stability for reconstitution into LCP, the T_m is no direct predictor for a suitable protein geometry or surface features that would enable efficient crystal packing. It is thus possible that a particular construct of a stabilized receptor does not crystallize due to unfavorable crystal packing. In this case, different chimeric constructs of the stabilized receptor have to be explored.

Comparison with other methods

The GPCR variants optimized through our modular platform can be directly applied to LCP-based structural biology pipelines with a high probability of success. The provided SLIC methodology offers an open-source, highly economic construct generation platform with a speed and success rate that is unmatched by current commercial DNA synthesis offers while being considerably cheaper.

While previously reported approaches for the screening and stabilization of GPCRs depend on the availability of modified ligands (fluorescently[14,16,17] or radioactively[8,18] labeled) or fusions to a fluorescent reporter protein[79,80], our CPM-based thermostabilization offers a more generic approach in that a ligand of choice can be used.

Compared with small-scale screening methods from baculovirus-infected *Sf9* insect cells[81]—a time-intensive undertaking that is difficult to parallelize—the small-scale high-throughput expression and subsequent microscale, magnetic bead-based purification from transiently transfected HEK293T cells enables a simultaneous preparation of many highly pure receptor variants within a single day and is thus ideally suited for automation.

However, by far the most unique feature of our CPM-based thermostabilization platform is its ability to yield GPCR variants that are specifically tailored for successful reconstitution and, hence, crystallization in LCP. While other engineering methods such as directed evolution[15,16] and

exhaustive scanning mutagenesis[8,18] also enable the generation of thermostabilized receptor variants, none of these methods has been directly predictive for successful crystallization, and they have therefore often entailed time- and resource-intensive campaigns to identify suitable crystallization constructs, methods and conditions through the process of crystallization itself.

Conclusions and possible future applications of the method

The described successful stabilization and screening methodology using the CPM assay as a sensitive readout and predictive tool to make GPCRs amenable for crystallization in LCP opens up exciting new possibilities for GPCR structural biology. The method allows for the rapid and cost-efficient thermostabilization of the receptor protein itself, independent of the number, nature or affinity of available labeled ligands for the receptor of interest. Therefore, receptors with no available radioactive or fluorescent high-affinity ligands can now be thermostabilized, which has remained a major limitation of all previously described thermostabilization approaches. It is thus now conceivable to stabilize and determine the crystal structures of orphan or odorant receptors. This avenue might be especially promising when used in conjunction with a preceding step of ligand-independent directed evolution towards higher functional expression levels[82].

Furthermore, the developed methodology might be especially valuable when combined with a recently reported computational approach for the prediction of stabilizing mutations in GPCRs[83]. Since the effect of the in silico-predicted single-point mutations and combinations thereof still has to be assessed experimentally, the integration of both methods might considerably accelerate the identification of suitable candidates for crystallization in LCP and the subsequent successful structure determination.

Although so far we have applied the CPM-based stabilization and screening approach only to GPCRs, in principle the methodology should be transferable to other membrane protein families that are compatible with crystallization in LCP[84].

Finally, the developed microscale purification method has the potential to become a highly versatile tool in the development of variants that allow the structure determination of membrane proteins, and thereby accelerate the whole process. While the purification method was initially developed and established as a manual workflow, the magnetic bead-based approach allows for full automatization of the procedure in a 96-well format when integrating automated magnetic particle processors, thereby decreasing hands-on time while further increasing the achievable throughput.

Importantly, the rapid and highly parallelizable purification method could also be used to prepare and screen samples for single-particle cryo-electron microscopy[85]. As more and more steps in cryo-electron microscopy workflows become automated (sample loading, deposition, vitrification, imaging and data processing), the bottleneck will invariably shift back towards the sample preparation stage[86]. Therefore, our method of membrane protein purification might become an attractive avenue to rapidly supply protein samples for structure determination. Especially the reduced shear forces during purification by avoiding long chromatographic procedures or extended immobilization times, the lack of protein concentrations steps, and the overall rapid purification process might allow the generation of high-quality samples of otherwise elusive, unstable membrane protein complexes.

Materials

Reagents

Generation of Ala/Leu scanning mutants

- Ethanol (EtOH; VWR International, cat. no. 20821.296, or equivalent)
- 2′-deoxyadenosine 5′-triphosphate (dATP), 100 mM solution (Thermo Fisher, cat. no. R0141, or equivalent); store at −20 °C
- 2× YT medium powder (Condalab, cat. no. 1507, or equivalent)
- Bacterial agar (Condalab, cat. no. 1802, or equivalent)
- Ampicillin (VWR International, cat. no. RC-020, or equivalent); store at −20 °C
- CutSmart buffer (New England Biolabs, cat. no. B7204); store at −20 °C
- NEBuffer 2.1 (New England Biolabs, cat. no. B7202); store at −20 °C
- dNTPs, 10 mM each (e.g., Thermo Fisher, cat. no. R0192); store at −20 °C
- Dimethyl sulfoxide (DMSO), anhydrous (Sigma Aldrich, cat. no. D8418, or equivalent); store desiccated
- Sodium acetate (Sigma Aldrich, cat. no. S2889, or equivalent)
- PCR product purification kit (e.g., Qiagen, cat. no. 28106)

- PCR product purification kit, 96-well format (e.g., Zymo Research, cat. no. D4023)
- Phusion high-fidelity buffer (New England Biolabs, cat. no. B0518); store at −20 °C
- Phusion high-fidelity DNA polymerase, 2 units per μl (New England Biolabs, cat. no. M0530); store at −20 °C
- Restriction enzyme HindIII-HF (New England Biolabs, cat. no. R3104); store at −20 °C
- Restriction enzyme NotI-HF (New England Biolabs, cat. no. R3189); store at −20 °C
- T4 DNA ligase buffer (Thermo Fisher, cat. no. B69); store at −20 °C
- T4 DNA polymerase (New England Biolabs, cat. no. M0203); store at −20 °C ▲ **CRITICAL** Heat-sensitive enzyme; handle stock at 4 °C maximum temperature.
- Chemically competent *E. coli* cells (e.g., strain DH5α); store at −80 °C
- Cloning vector pcDNA5 SLIC; store at −20 °C
- Forward mutagenesis primers, 10 μM solution; store at −20 °C
- Forward vector primer, 100 μM solution; store at −20 °C
- Reverse mutagenesis primers, 10 μM solution; store at −20 °C
- Reverse vector primer, 100 μM solution; store at −20 °C

Transient transfection of mammalian cells with GPCR constructs
- Dulbecco's modified Eagle's medium (DMEM; Sigma Aldrich, cat. no. D6429)
- Dulbecco's phosphate buffered saline (DPBS; Sigma Aldrich, cat. no. D8537)
- Fetal calf serum (BioConcept, cat. no. 2-01F30-I):
- Opti-MEM I medium (Thermo Fisher, cat. no. 31985062)
- Penicillin–streptomycin solution (Sigma Aldrich, cat. no. P4333)
- Na-butyrate (Sigma Aldrich, cat. no. 303410)
- TransIT-293 transfection reagent (Mirus, cat. no. MIR2705)
- HEK293T/17 cells (ATCC no. CRL-11268)

Microscale solubilization and purification of GPCR constructs
- *n*-Dodecyl-β-D-maltopyranoside (DDM; Anatrace, cat. no. D310)
- Cholesteryl hemisuccinate (CHS; Sigma Aldrich, cat. no. C6512)
- Adenosine 5′-triphosphate (ATP; Sigma Aldrich, cat. no. 2383)
- 3× FLAG peptide (Sigma Aldrich, cat. no. F4799)
- Anti-FLAG M2 magnetic beads (Sigma Aldrich, cat. no. M8823)
- Deoxyribonuclease I (DNase I) (Sigma Aldrich, cat. no. DN25)
- Iodoacetamide (Sigma Aldrich, cat. no. I1149)
- 4-(2-hydroxyethyl)-1-piperazineethanesulfonic acid (HEPES; ITW Reagents, cat. no. A1069, or equivalent)
- KCl (Sigma Aldrich, cat. no. P9541, or equivalent)
- NaCl (Sigma Aldrich, cat. no. S9888, or equivalent)
- $MgCl_2$ (Sigma Aldrich, cat. no. M8266, or equivalent)
- Pefabloc SC (Carl Roth, cat. no. A154.1, or equivalent)
- Pepstatin A (Carl Roth, cat. no. 2936.3, or equivalent)

Determination of the apparent T_m of purified GPCR constructs
- CPM dye (Sigma Aldrich, cat. no. C1484)

Equipment

Design of SLIC PCR primers
- Spreadsheet software (e.g., Microsoft Office Excel, Microsoft)
- DNA analysis software (e.g., CLC Main Workbench, Qiagen)

Generation of Ala/Leu scanning mutants
- 0.2 ml PCR tubes
- 1.5 ml microcentrifuge tubes
- 12-channel multichannel pipette
- Six-well tissue culture dish (e.g., Corning, cat. no. 353046)
- 96-well PCR microplates (e.g., Axygen, cat. no. PCR-96-FS-C)
- 96-well PCR thermal cycler (e.g., TProfessional BASIC 96 Gradient, Biometra)

- 96-well V-bottom plates (e.g., Sigma-Aldrich, cat. no. 651201)
- Absorbent paper
- Adhesive plate seals (e.g., Thermo Fisher, cat. no. AB-0580)1
- Aluminum microplate sealing film (e.g., Axygen, cat. no. PCR-AS-200)
- Gas-permeable adhesive plate seals (e.g., 4titude, cat. no. 4ti-0517)
- Ice bucket
- Metal block for 1.5 ml microcentrifuge tubes and 96-well PCR microplates
- Multistep dispenser (e.g., Multipette M4, Eppendorf)
- Plating beads (e.g., Merck, cat. no. 71013)
- Refrigerated benchtop centrifuge, up to 20,000*g* (e.g., Centrifuge 5430 R, Eppendorf)
- Temperature-controlled block for microcentrifuge tubes (e.g., Thermomixer comfort, Eppendorf)
- Vortex mixer (e.g., Vortex-Genie 2)

Transient transfection of mammalian cells with GPCR constructs

- 10 and 50 ml conical tubes
- 2 ml microcentrifuge tubes
- Six-well tissue culture dishes (e.g., Corning, cat. no. 353046)
- Absorbent paper
- Benchtop centrifuge (e.g., Centrifuge 5430 R, Eppendorf)
- Cell counter (e.g., CASY cell counter)
- Class II biological safety laminar flow hood
- Humidified CO_2 tissue culture incubator
- T75 tissue culture flask (e.g., TPP, cat. no. 90076)
- Vortex mixer (e.g., Vortex-Genie 2)

Microscale solubilization and purification of GPCR constructs

- 1.5 and 2 ml microcentrifuge tubes
- 10 and 50 ml conical tubes
- 12-channel multichannel pipette
- Ice bucket
- Low-retention pipette tips
- Magnetic separator (e.g., DynaMag-2 Magnet, Thermo Fisher Scientific)
- Metal block for 1.5 and 2.0 ml microcentrifuge tubes
- Multistep dispenser (e.g., Multipette M4, Eppendorf)
- Refrigerated benchtop centrifuge, capable of 20,000*g* (e.g., Centrifuge 5430 R, Eppendorf)
- Small-tube rotor
- Vortex mixer (e.g., Vortex-Genie 2)

Determination of the apparent T_m of purified GPCR constructs

- 12-channel multichannel pipette
- 96-well semi-skirted quantitative PCR (qPCR) microplate (e.g., Thermo Scientific, cat. no. AB1400W)
- 96-well skirted PCR microplate (e.g., Corning, cat. no. 6511)
- Adhesive sealing foil for qPCR microplates (e.g., Roche LightCycler 480 Sealing Foil, cat. no. 04729757001)
- Benchtop centrifuge equipped with plate rotor (e.g., Centrifuge 5430 R, Eppendorf)
- Ice bucket
- Low-retention pipette tips
- Metal block for 1.5 and 2.0 ml microcentrifuge tubes
- Metal block for 96-well PCR plates
- qPCR thermal cycler system with suitable excitation and emission filters (e.g., Agilent Mx3005p equipped with ANS filter set)
- Vortex mixer (e.g., Vortex-Genie 2)

Reagent setup

2× YT medium

2× YT nutrient medium prepared according to manufacturer's instructions. Autoclave, and store at room temperature (RT, 20–25 °C) for a maximum of 6 months.

2× YT growth medium
2× YT recovery medium supplemented with appropriate antibiotic (e.g., 100 μg/ml ampicillin). Store at RT for up to 2 weeks.

2× YT six-well counter-selection agar plates
Add 1.5 g of bacterial agar per 100 ml 2× YT medium before autoclaving. Add appropriate antibiotic (e.g., 100 μg/ml ampicillin) and 7% sucrose (wt/vol) to the cooling agar solution. Per well of the six-well plate, add 2 ml of the molten agar mixture. Store plates at 4 °C for up to 4 weeks.

PCR template solution
PCR template plasmid (e.g., pcDNA5_NK1R-y04) is diluted to 0.1 ng/μl. Use only freshly prepared plasmid dilutions.

70% EtOH
Prepare a 70% (vol/vol) EtOH solution in water. Store and use at −20 °C.

70% (wt/vol) sucrose solution
Dissolve 70 g of sucrose in 100 ml of water. Filter-sterilize the solution with a 0.22 μm filter. Store at RT for a maximum of 6 months.

Ampicillin solution
For a 1,000× stock solution, dissolve 100 mg ampicillin in 1 ml of water. Filter-sterilize the solution with a 0.22 μm filter, and store in aliquots at −20 °C for a maximum of 2 years.

DNA precipitation buffer
3 M sodium acetate dissolved in water and titrated to pH 5.2 with HCl. Store at RT for a maximum of 2 years.

Sterile distilled water
Filter-sterilize water with a 0.22 μm filter.

Complete DMEM
To prepare complete medium, add 50 ml fetal calf serum and 5 ml penicillin–streptomycin solution to 500 ml DMEM in a laminar flow hood. Store the complete medium at 4 °C for a maximum of 4 weeks.

Na-butyrate solution
Prepare a 0.5 M solution in water. Filter-sterilize the solution with a 0.22 μm filter, and store at RT for a maximum of 1 year.

3× FLAG peptide
Prepare a 3 mg/ml solution in 50 mM HEPES pH 7.5, 150 mM NaCl. Store aliquots at −20 °C.

ATP solution
Prepare a 250 mM solution in 50 mM HEPES pH 7.5. Store in aliquots at −80 °C.

Anti-FLAG M2 magnetic beads
Prepare 20 μl slurry aliquots, and store at −20 °C to prevent freeze–thaw cycles.

Bead-resuspension buffer
Prepare a solution of 25 mM HEPES pH 7.5, 150 mM NaCl. Prepare fresh for each experiment.

DNase I solution
Prepare a 25 mg/ml solution in 10 mM HEPES pH 8.0, 150 mM NaCl, 1 mM $MgCl_2$, 50% (vol/vol) glycerol. Store in aliquots at −20 °C for a maximum of 1 year.

Iodoacetamide solution
Dissolve 100 mg/ml in 50 mM Tris pH 7.4 (titrated at RT). Prepare immediately before use.

DDM/CHS
Prepare a 10%/2% (wt/vol) stock solution in 200 mM Tris pH 8.0 (titrated at RT). First dissolve DDM, then incorporate CHS using sonication. Store at 4 °C for a maximum of 2 months.

Hypotonic buffer (low salt)
Prepare a solution of 10 mM HEPES pH 7.5, 20 mM KCl, 10 mM $MgCl_2$, 50 μg/ml Pefabloc SC, 1 μg/ml Pepstatin A, 0.2 mg/ml DNase I. Prepare fresh for each experiment. ▲ **CRITICAL** Ligand has to be added at an appropriate concentration.

2× Solubilization buffer
Prepare a solution of 25 mM HEPES pH 7.5, 1.0 M NaCl, 1%/0.2% DDM/CHS (wt/vol). Prepare fresh for each experiment. ▲ **CRITICAL** The exact buffer composition, e.g., NaCl and/or DDM/CHS concentration, may have to be optimized for each GPCR.

Wash buffer 1
Prepare a solution of 50 mM HEPES pH 7.5, 500 mM NaCl, 10 mM $MgCl_2$, 10% (vol/vol) glycerol, 0.25%/0.05% (wt/vol) DDM/CHS, 8 mM ATP. Prepare fresh for each experiment. ▲ **CRITICAL** The exact buffer composition may have to be optimized for each GPCR. Ligand has to be added at an appropriate concentration, depending on its K_D, solubility, availability and cost. If possible, it should be added at a concentration saturating the receptor.

Wash buffer 2
Prepare a solution of 50 mM HEPES pH 7.5, 500 mM NaCl, 10% (vol/vol) glycerol, 0.05%/0.01 (wt/vol) DDM/CHS. Prepare fresh for each experiment. ▲ **CRITICAL** The exact buffer composition may have to be optimized for each GPCR. Ligand has to be added at an appropriate concentration.

Elution buffer
Prepare a solution of 25 mM HEPES pH 7.5, 500 mM NaCl, 10% (vol/vol) glycerol, 0.05%/0.01 (wt/vol) DDM/CHS, 300 μg/ml 3× FLAG peptide. Prepare fresh for each experiment. ▲ **CRITICAL** The exact buffer composition may have to be optimized for each GPCR. Ligand has to be added at an appropriate concentration.

CPM dye solution
Prepare a 4 mg/ml (9.94 mM) solution in DMSO. Prepare 2.5 μl aliquots, store at −80 °C away from light exposure for a maximum of 2 years.

Dilution buffer
Prepare a solution of 25 mM HEPES pH 7.5, 500 mM NaCl, 10% (vol/vol) glycerol, 0.05%/0.01 (wt/vol) DDM/CHS. Prepare fresh for each experiment.

Procedure

Primer design for SLIC

▲ **CRITICAL** In SLIC, circular plasmids are assembled from linearized vector and insert fragments. The efficiency of the method critically depends on the quality of the insert fragments generated by PCR. A robust design of the PCR primers is thus of central importance for a successful application of the method. Here we describe the empirically determined requirements for the design of reliable primers. Every primer has to meet two criteria: (i) a DNA melting temperature >52 °C of the primer part that is annealing during the first PCR cycle and (ii) an overhang homologous to the adjacent fragment or to the vector of ~30 bp. The DNA melting temperature (T_m) in °C is calculated according to Eq. 1:

$$Tm = 64.9 + 41 * \frac{(y * G + z * C - 16.4)}{(w * A + x * T + y * G + z * C)} \quad (1)$$

Here w, x, y and z are the numbers of the bases A, T, G and C in the sequence, respectively. The actual primer melting temperature in the PCR mixture is higher than approximated by the above equation (>60 °C) since salt and primer concentrations are not accounted for in the equation (actual primer melting temperatures can be better estimated using the manufacturer's online calculator at

https://www.thermofisher.com/ch/en/home/brands/thermo-scientific/molecular-biology/molecular-biology-learning-center/molecular-biology-resource-library/thermo-scientific-web-tools/tm-calculator.html). Nevertheless, we based our primer design on the melting temperature approximated by the above equation, since it allowed the most reliable prediction of a successful PCR and freely available software can be used for melting temperature calculation (e.g., basic T_m calculation tool on http://insilico.ehu.es).

Vector primer design ● Timing 1 h

▲ **CRITICAL** Oligonucleotide primers are required to introduce to the GOI the overhangs that are homologous to the target vector ('vector primers') (Fig. 4b). Hence, the identical vector primer pair is used in all SLIC-based construct generation and mutagenesis procedures of a given vector–GOI combination. It is thus important to obtain these primers in sufficient amounts (>0.02 μmol) and quality. Vector primers typically have a length of ~50 bp.

1 Construct the desired expression vector containing the GOI in silico using a DNA analysis software (Fig. 4a).

2 Design a forward vector primer introducing an overhang homologous to the vector upstream of the GOI: in the coding strand of the GOI, starting at the 5′-end, select a sequence with a DNA melting temperature >52 °C according to Eq. 1.

3 Elongate this sequence by 30 bp in the 5′-direction into the vector sequence to obtain the forward vector primer. Copy the primer sequence into your database.
▲ **CRITICAL STEP** Primer length should not exceed 60 bp to ensure efficient PCR amplification. If the primer length exceeds 60 bp, choose a homologous overhang shorter than 30 bp (but at least 20 bp).

4 Design a reverse vector primer analogously, introducing an overhang homologous to the receptor downstream of the GOI: in the non-coding strand of the GOI, starting at its 5′-end, select a sequence with a DNA melting temperature >52 °C.

5 Elongate this sequence by 30 bp in the 5′-direction into the vector sequence to obtain the reverse vector primer. Copy the primer sequence into your database.
▲ **CRITICAL STEP** Primer length should not exceed 60 bp to ensure efficient PCR amplification. If the primer length exceeds 60 bp, choose a homologous overhang shorter than 30 bp (but minimally 20 bp).

6 Obtain vector primers from a DNA synthesis company (e.g., Integrated DNA Technologies). Dissolve lyophilized primers to a concentration of 100 μM in water.
▲ **CRITICAL STEP** Typically, vector primers are obtained at standard desalted grade, but depending on the DNA synthesis provider the quality may drastically decrease with primer length. Thus, vector primer quality should be assessed by DNA sequencing of a small number of test cloning reactions with respect to the mutation rate in the primer region. If necessary, primers have to be procured at a higher purity grade or from a different supplier.

Design of SLIC mutagenesis primer pairs ● Timing 1 d

▲ **CRITICAL** As depicted in Fig. 4b, for every desired mutant a specific pair of mutagenesis primers is designed. The mutation is introduced by generating an N- and C-terminal fragment of the GOI by PCR amplification with a mutagenesis and a vector primer. Mutagenesis primers should be obtained as predissolved 10 μM solutions in a 96-well plate format (available from, e.g., Integrated DNA Technologies) at standard desalted grade. Ideally, forward and reverse mutagenesis primers should be located on separate plates, with primer pairs in identical well positions to facilitate preparation of the mutagenesis reactions. Mutagenesis primers typically have a length of ~35 bp.

7 Introduce the desired mutation in the sequence of the GOI in silico using a standard DNA analysis software. Exchange the entire codon of the target amino acid for a defined mutated codon (e.g., GCC for Ala, CTG for Leu).

8 Design of forward mutagenesis primer: on the coding strand, go to the 3′-end of the mutant codon and, in the 3′-direction, select a sequence with a DNA melting temperature >52 °C.

9 Elongate this sequence by 17 bp (3 bp for the mutant codon plus 14 bp) in the 5′-direction to obtain the forward mutagenesis primer. Copy the primer sequence into your database.

10 Design the reverse mutagenesis primer analogously: on the noncoding strand, go to the 3′-end of the mutant codon and, in the 3′-direction, select a sequence with a DNA melting temperature >52 °C.

11 Elongate this sequence by 17 bp (3 bp for the mutant codon plus 14 bp) in the 5′-direction to obtain the reverse mutagenesis primer. Copy the primer sequence into your database.
12 Change mutant codon back to wild type in the DNA analysis software, and repeat Steps 7–12 for the next mutant.

Design of fusion protein assembly primer pairs ● Timing 1 d

▲ **CRITICAL** In this step, the hydrophilic fusion partner is inserted, typically into ICL3. Fusion protein assembly primers are designed on the GOI with overhangs homologous to the fusion protein (Fig. 4b). Thus, different fusion proteins can be conveniently ordered directly as synthesized double-stranded DNA blocks, which can be used without further modification. Fusion assembly primers typically have a length of ~50 bp.

13 Construct the desired GOI-fusion protein sequence in silico using a DNA analysis software.
14 Design of forward fusion assembly primer: on the coding strand, start at the 3′-end of the fusion protein insertion and, in the 3′-direction, select a sequence with a DNA melting temperature >52 °C.
15 Elongate this sequence by 30 bp in the 5′-direction into the fusion protein sequence to obtain the forward fusion assembly primer. Copy the primer sequence into your database.
▲ **CRITICAL STEP** Primer length should not exceed 60 bp to ensure efficient PCR. If the primer length exceeds 60 bp, choose a homologous overhang shorter than 30 bp (but minimally 20 bp).
16 Design the reverse fusion assembly primer analogously: on the noncoding strand, start at the 3′-end of the fusion protein insertion and, in the 3′-direction, select a sequence with a DNA melting temperature >52 °C.
17 Elongate this sequence by 30 bp in the 5′-direction into the fusion protein sequence to obtain the reverse fusion assembly primer. Copy the primer sequence into your database.
▲ **CRITICAL STEP** Primer length should not exceed 60 bp to ensure efficient PCR. If the primer length exceeds 60 bp, choose a homologous overhang shorter than 30 bp (but minimally 20 bp).

Generation of Ala/Leu scanning mutants ● Timing 2–3 weeks

▲ **CRITICAL** In this example, the modified NK1R gene is inserted into a modified high-copy-number pcDNA5 vector for mammalian expression, resulting in pcDNA5_NK1R-y04 (Fig. 4a). Thus, the expressed receptor is N-terminally fused to a melittin signal sequence, followed by a FLAG epitope, a His_{10} tag and a TEV protease cleavage site. Adjustments to the protocol are required for vectors of different size, antibiotic resistance or copy number.

▲ **CRITICAL** Although insert fragments after single-stranded DNA overhang generation by T4 DNA polymerase treatment can be stored for extended time periods at −20 °C and reused after thawing, it is highly recommended to prepare the inserts fresh for maximal efficiency of the method. For users unfamiliar with the SLIC procedure, it is highly recommended to start with a subset of mutants to get familiar with the protocol.

18 Linearize the cloning vector by restriction enzyme digestion. Add 120 µg of vector pcDNA5 SLIC, 100 µl CutSmart buffer, 24 µl restriction enzyme HindIII-HF (480 units), 24 µl restriction enzyme NotI-HF (480 units) and water to a total volume of 1 ml in a 1.5 ml microcentrifuge tube. Incubate for 5 h at 37 °C.
19 Purify linearized cloning vector using a commercially available PCR product purification kit. Elute in a total volume of 600 µl of the supplied elution buffer.
▲ **CRITICAL STEP** Consider the loading capacity of the purification column (as indicated by the vendor), and use several columns if necessary. DNA concentration after elution should be ≥80 ng/µl.
20 Add 50 µg of linearized cloning vector to 100 µl NEBuffer 2.1 and 8.3 µl T4 DNA polymerase (24.9 units) in a total volume of 1 ml in a 1.5 ml microcentrifuge tube. Incubate for 30 min at 23 °C.
▲ **CRITICAL STEP** Meet the exact incubation time of 30 min to ensure that the single-stranded overhangs have the optimal length for efficient annealing and subsequent DNA repair.
21 Add 10 µl 100 mM dATP stock solution to stop the exonuclease digest, and mix by pipetting up and down. Transfer to a precooled metal block on ice. Prepare 50 µl aliquots in 0.2 ml PCR tubes, and store at −20 °C until further use.
■ **PAUSE POINT** The samples can be stored at −20 °C for several days.
22 Prepare two separate PCR reaction mixtures for the N-terminal fragments (containing forward vector primer) and the C-terminal fragments (containing reverse vector primer) as follows:

Component	Volume per reaction (µl)
Phusion HF buffer	10
dNTPs	1
Vector primer (forward or reverse)	0.5
PCR template plasmid	1
DMSO	1.5
Phusion DNA polymerase	0.5
Water	30.5
Total volume	50

23 Add 45 µl of the PCR reaction mixture and 5 µl of mutagenesis primer to a 96-well PCR microplate using a multichannel pipette. Prepare separate plates for N-terminal fragments (add reverse mutagenesis primers) and C-terminal fragments (add forward mutagenesis primers). Seal plates with aluminum microplate sealing film.

24 Transfer plates into a 96-well PCR thermal cycler, and run the following cycle with a minimal elongation time of 30 s:

Cycle number	Denaturing	Annealing	Elongation
1	98 °C, 1 min		
2–36	98 °C, 10 s	60 °C, 20 s	72 °C, 20 s/kbp
37			72 °C, 5 min

■ **PAUSE POINT** The samples can be stored at −20 °C for several days.

25 Purify amplified N- and C-terminal fragments separately using a commercially available 96-well format PCR product purification kit following the manufacturer's instructions. Elute the purified PCR products in 30 µl of the supplied elution buffer.

▲ **CRITICAL STEP** DNA concentration should be ≥80 ng/µl. Additionally, to verify PCR product quality, 5 µl of purified product can be analyzed by electrophoresis on a 0.8% agarose gel.

■ **PAUSE POINT** The samples can be stored at −20 °C for several days.

26 Prepare a reaction mixture consisting of 2 µl NEBuffer 2.1, 0.17 µl T4 DNA polymerase (0.51 units) and 7.83 µl water per reaction in a 1.5 ml microcentrifuge tube. Mix by pipetting up and down.

27 Add 10 µl reaction mixture to each well of a 96-well PCR microplate using a multistep dispenser. Add 10 µl per well PCR fragment using a multichannel pipette, and mix by pipetting. Seal plate with adhesive plate seal, and incubate for 30 min at 23 °C.

▲ **CRITICAL STEP** Meet the exact incubation time of 30 min.

28 Add 2 µl per well 10 mM dATP (1:10 dilution of 100 mM stock in water), and mix by pipetting up and down. Transfer plate to a precooled metal block on ice.

29 Thaw an adequate number of aliquots of linearized cloning vector with single-stranded DNA overhangs on ice. Add 5 µl per well vector to each well of a new 96-well PCR microplate.

30 Add 2 µl per well of a 1:1 dilution of T4 DNA ligase buffer in water using a multichannel pipette.

31 Add 1.5 µl per well N-terminal fragment and 1.5 µl per well C-terminal fragment using a multichannel pipette. Mix by pipetting, and seal plate with aluminum microplate sealing film. Anneal vector and fragments by incubation for 30 min at 37 °C in a 96-well PCR thermal cycler.

32 Per reaction, thaw 20 µl of chemically competent *E. coli* cells in a precooled metal block on ice. Add 20 µl competent cells to each well of a precooled 96-well PCR microplate in a metal block on ice.

33 Add 2 µl per well of annealing mixture to competent cells using a multichannel pipette. Seal plate with adhesive plate seal, and incubate for 30 min on ice.

▲ **CRITICAL STEP** Shorter incubation time results in decreased transformation efficiency.

34 Transfer plate to a 96-well PCR thermal cycler, and transform the cells with the plasmid by incubation at 42 °C for 1 min. After the heat shock, immediately transfer the plate back to the metal block on ice and incubate for 2 min.

35 Add 30 µl of 2× YT recovery medium per well to transformed cells. Seal plate with adhesive plate seal and incubate for 30 min at 37 °C in an incubator. Resuspend cells by gently pipetting up and

down with a multichannel pipette, and plate out 20 µl cell suspension on six-well counter-selection agar plates using glass beads. Incubate overnight at 37 °C in an incubator.

■ **PAUSE POINT** The agar plates can be stored at 4 °C for several days.

36 Add 250 µl 2× YT growth medium to a 96-well V-bottom plate. Pick a single colony of each mutant, and place it into a single well of the plate. Incubate for 4 h at 37 °C.

37 Prepare sequencing cultures according to the service providers' (e.g., Microsynth) instructions from the preculture obtained in Step 36. Sequence each mutant using both standard primers CMV-for and BGH-rev.

▲ **CRITICAL STEP** Complete sequencing of the entire insert in the vector is essential to ensure integrity of the plasmid. If plasmid preparation is performed by the sequencing provider, ask the sequencing provider to ship the prepared plasmid to you after sequencing.

■ **PAUSE POINT** The plasmid samples can be stored at −20 °C for several days.

38 Precipitate the plasmid DNA to remove residual endotoxin. Per 100 µl of plasmid solution in a 1.5 ml microcentrifuge tube, add 10 µl DNA precipitation buffer and 200 µl 100% EtOH. Mix by inverting the tube, and incubate at −20 °C for ≥4 h.

■ **PAUSE POINT** The samples can be stored at −20 °C for several days.

39 Centrifuge for 30 min at 20,000*g* in a refrigerated benchtop centrifuge precooled to 4 °C. Decant the supernatant.

40 Wash the DNA pellet by adding 1 ml 70% EtOH precooled to −20 °C and subsequent centrifugation at 20,000*g* for 15 min at 4 °C. Repeat the washing step one more time.

41 Decant the supernatant, and tap the tube on absorbent paper to remove any residual EtOH. Dry the DNA pellet for 20 min at 40 °C in a temperature-controlled block for microcentrifuge tubes (keep the tube lid open). Add 50 µl of sterile-filtered water to dissolve the plasmid DNA.

Transient transfection of mammalian cells with GPCR constructs ● Timing 2–3 d

▲ **CRITICAL** The steps below have been optimized for expressing the yeast-evolved human NK1R mutant NK1R-y04 or mutants thereof in the pcDNA5_NK1R-y04 format (Fig. 4a). Even though this standard procedure has been successfully applied to most tested GPCRs, prior optimization of this step for each target GPCR is highly recommended. Parameters that may need to be optimized include the number of wells used for each mutant (typically one to three, depending on the expression level of the specific target GPCR), the transfection reagent, the transfected amount of plasmid (0.5–1.5 µg), the possible addition of Na-butyrate and the time before harvesting the cells (48–72 h).

42 Seed 7.5×10^5 HEK293T cells in 2 ml DMEM per well of a six-well plate, using sufficient plates for the number of mutants or constructs to be expressed. Grow the cells for 20–24 h at 37 °C in a humidified 5% (vol/vol) CO_2 atmosphere.

43 Transfect cells of each well by adding 262.5 µl of transfection mixture, consisting of 1.5 µg of plasmid DNA (prepared at 300 ng/µl) in 250 µl Opti-MEM I and 7.5 µl TransIT-293. Incubate the cells with transfection mixture for 24 h.

44 Exchange medium with 2 ml fresh DMEM containing 5 mM Na-butyrate. Incubate the cells for 48 h at 37 °C in a humidified 5% (vol/vol) CO_2 atmosphere.

45 To harvest the cells, rinse them off the plate using the growth medium and transfer them into a 2 ml microcentrifuge tube. Centrifuge (500*g*, 5 min) and decant the supernatant carefully. Gently resuspend the cells in 1 ml DPBS, and repeat the centrifugation step.

46 Decant the supernatant, and tap the tube on absorbent paper to remove any residual DPBS.

47 Cell pellets can now be stored at −20 °C for extended time periods.

Microscale solubilization and purification of GPCR constructs ● Timing 7–8 h

▲ **CRITICAL** This section describes the solubilization and purification of antagonist-bound, yeast-evolved NK_1R[17], which has increased expression levels, is stable during purification and displays monodisperse behavior on size-exclusion chromatography. The provided steps might require optimization for a given new GPCR, depending on the actual yields and stability during solubilization and purification of the expressed receptor (please see Table 1 for further advice). Parameters to be varied include the initial solubilization volume (depending on the number of cells required to obtain sufficient amounts of purified protein), the ligand and its concentration to be used during purification (a function of its affinity and solubility), and the buffer compositions, as well as the concentration and type of detergent.

▲ **CRITICAL** Up to 30 mutants or constructs can be purified in parallel using the protocol below. Ideally, an optimized purification protocol is established beforehand with regard to the above-mentioned parameters

to scout for expression levels of constructs and especially check for protein monodispersity in aSEC. This initial assessment and optimization can be performed using fluorescence-detection size-exclusion chromatography by genetically fusing the candidate GPCR to GFP or other fluorescent proteins[79,87].

48 Thaw HEK293T cell pellets (in 2 ml microcentrifuge tubes) on ice for 10 min.

49 Add 125 µl ice-cold hypotonic buffer containing ligand (e.g., 250 µM CP-99,994) to each tube. Incubate on ice for 15 min, and vortex vigorously several times to ensure homogeneous resuspension and lysis of cells.

50 Add 5 µl of iodoacetamide solution to each tube to alkylate surface-exposed thiol groups. Incubate on ice for 15 min with vigorous vortexing from time to time.

51 Carefully transfer solution from 2 ml tubes into 1.5 ml microcentrifuge tubes.

52 Add 130 µl 2× solubilization buffer to each tube. Transfer tubes to a small-tube rotor for solubilization for 1 h at 4 °C.

▲ **CRITICAL STEP** The temperature and duration of solubilization has to be optimized for each GPCR.

53 During the incubation time in Step 52, prepare anti-FLAG M2 magnetic beads by thawing frozen 20 µl slurry aliquots at RT. Wash the slurry by adding 500 µl bead-resuspension buffer, centrifuge briefly at 500*g*, place tubes in a magnetic separator to collect the beads, aspirate and discard the supernatant. Repeat the washing step one more time, and place the washed resin on ice.

54 Centrifuge the solubilization mixture at 20,000*g* for 30 min at 4 °C.

55 Add the supernatant containing solubilized protein to the prepared anti-FLAG M2 magnetic beads.

▲ **CRITICAL STEP** If the pellet of unsolubilized material appears to be soft, remove it by aspirating it using a small pipette tip before transfer of the supernatant.

56 Incubate the samples for 3 h on a small-tube rotor at 4 °C. Meanwhile, prepare wash and elution buffers and incubate all buffers on ice.

57 Centrifuge samples at 500*g* for 3 min at 4 °C.

58 Place tubes in the magnetic separator to collect the beads, and remove the supernatant with a pipette. Remove tubes from the magnetic separator, and place tubes in a metal block on ice.

59 Add 250 µl wash buffer 1, and incubate for 3–4 min until the magnetic beads have been collected at the bottom of the tubes. Place the tubes in the magnetic separator, and remove supernatant as described before.

▲ **CRITICAL STEP** Do not try to resuspend the beads by pipetting or inverting the tube; it is possible for the magnetic beads to stick to the pipette tip or tube lid.

60 Repeat Step 59 using wash buffer 1.

61 Add 250 µl wash buffer 2, and proceed as during Step 59.

62 Repeat Step 61 two times using wash buffer 2.

63 After the final washing step, ensure complete removal of any residual wash buffer 2 by visual inspection and, if needed, additional aspiration of residual solution.

64 For elution, gently detach the beads located at the side of the tubes with 23 µl elution buffer. Incubate on ice for 15 min.

65 Mix the elution solution by carefully pipetting up and down using a low-retention pipette tip. Incubate on ice for a further 15 min.

66 During the incubation time, perform Steps 69 and 70.

67 Carefully remove 21 µl of supernatant containing the purified GPCR and transfer to a fresh 1.5 ml microcentrifuge tube.

▲ **CRITICAL STEP** It is essential to ensure removal of supernatant without carry-over of any magnetic beads. Therefore, place the tubes in the magnetic separator and visually check proper collection of the magnetic beads at the sidewall of the tubes.

68 Centrifuge collected supernatant at 20,000*g* for 5 min at 4 °C, and place tubes on ice. Immediately proceed with Step 71.

Determination of the apparent T_m of purified GPCR constructs ● Timing 1.5 h

▲ **CRITICAL** This section was optimized for the determination of the apparent T_m of various GPCRs purified in DDM/CHS using the fluorescent dye CPM in combination with an Agilent Mx3005p qPCR system using an excitation wavelength of 330 nm and a detection wavelength of 490 nm.

▲ **CRITICAL** Ideally, a total of 0.5–2 µg of GPCR in the final reaction volume of 20 µl is assayed under the described conditions (corresponding to a protein concentration in the final reaction volume of 0.5–2 µM, assuming a molecular weight of 50 kDa). Under these conditions, the assay is in its lower linear range, which is important because any changes in expression level and purification efficiency will

translate directly into different signal amplitudes, allowing construct ranking based on the additional criterion of the amount of purified protein. The CPM dye is initially dissolved at 4 mg/ml in DMSO (9.94 mM). Thus, in the described setup, the final concentration of dye during measurement is 24.8 µM.

69 Start the qPCR system to allow for the 30 min heating phase of the lamp before performing measurements. Program the qPCR machine with the following protocol: 5 min equilibration at 25 °C, followed by a 2 °C/min thermal ramp from 25 °C to 90 °C.

70 Thaw a CPM dye aliquot at RT in the dark, and dilute 1:40 with dilution buffer that has been prewarmed to RT. Ensure proper dilution and mixing of the dye by vortexing the solution several times.
▲ **CRITICAL STEP** Store the solution in the dark at RT. We typically store it in a rack that is placed in a drawer.

71 Add 2 µl of the prepared CPM dye solution from Step 70 to the appropriate number of wells of a 96-well PCR microplate, and subsequently put the plate on ice.
▲ **CRITICAL STEP** Discard remaining dye solution, as the dye will degrade. Do not reuse.

72 Transfer 18 µl of purified GPCR sample to each well using a low-retention pipette tip; mix carefully.
▲ **CRITICAL STEP** Pipetting must be performed accurately, and formation of air bubbles should be avoided.

73 Transfer 19.5 µl of the mixed samples to a 96-well qPCR microplate at RT using a multichannel pipette.
▲ **CRITICAL STEP** Manually inspect all wells for air bubbles. If detected, a quick centrifugation step at 500*g* can be performed.

74 Seal the plate thoroughly with adhesive sealing foil. Place the qPCR plate in the heating block of the qPCR system, and close the lid of the heating block.

75 Start the above-described qPCR protocol. After the run has finished, save and export the results for analysis.

76 Analyze the fluorescence signal (Y) versus temperature (T) data, and determine the apparent T_m of each mutant or construct by fitting to the data a sigmoidal equation,

$$Y = Y_0 + \frac{(Y_{max} - Y_0)}{1 + \exp\left(\frac{T_m - T}{slope}\right)} \quad (2)$$

Y_0 and Y_{max} correspond to the baseline and the signal at saturation, respectively, whereas the empirical parameter *slope* accounts for the different steepness of melting curves. Fitting can be performed, e.g., in GraphPad Prism. For easy visual comparison, the melting curves can be normalized (Fig. 2b,c). Rank the constructs according to their $\Delta T_m = T_{m,wild-type} - T_{m,mutant}$

77 As the maximal attainable fluorescence amplitude, $\Delta Y = Y_{max} - Y_0$, depends on the amount of protein in the reaction mixture, a rough idea about overall expression and purification yield can be obtained by comparing ΔY between constructs. This qualitative comparison has proven to be helpful during screening of different fusion constructs for crystallization in LCP.

Combining thermostabilizing mutations to obtain optimally stabilized GPCR mutants

● **Timing 6–8 weeks**

▲ **CRITICAL** To achieve a T_m of ~60 °C, it is typically necessary to combine several thermostabilizing mutations. Care should be taken to analyze each beneficial single-point mutation identified during initial screening with regard to its influence on purification yield as well as its location in the possible tertiary structure (i.e., helical interfaces).

▲ **CRITICAL** Beneficial mutations that are directly opposing each other in a helix–helix interface should be identified; in each combinatorial study, use only one of these to avoid steric interference.

▲ **CRITICAL** The results of the initial screening might vary widely in number of mutants and detected ΔT_m values. Therefore, to limit the number of combinatorial constructs but ensure proper screening and success in thermostabilization, a lower cutoff value based on relative ΔT_m should be chosen.

78 Identify the most thermostable single-point mutation (mutant A) from the initial screening results as a starting point for making the double mutants. Construct all possible double mutants of mutant A with each of the 10–15 next most thermostable mutations (based on a ΔT_m cutoff value, e.g., 2 °C) by using the available SLIC primers according to the provided protocol with the DNA of mutant A as the template.
▲ **CRITICAL STEP** Initially perform in silico cloning to ensure that the intended primers for combinatorial studies do not overlap with the mutation of mutant A, and if they do, design and order new primers.

79 Perform SLIC mutagenesis, transient transfections, expression, purification and apparent T_m determination as initially established for the GPCR to determine the apparent T_m of each double mutant.
80 Identify the double mutant for which the combination of mutations shows the highest additive effect, i.e., leads to the strongest increase in apparent T_m.
81 Repeat Steps 78–80 to create triple mutants based on the best double mutant. Only add mutations that have shown additive effects during screening of the double mutants. This step can be expanded by including the second- and third-ranked double mutants as starting points for triple mutants as well.
82 Repeat this process until a sufficiently thermostable mutant is identified in the CPM-based assay, which displays an apparent T_m around or above 60 °C.
83 As soon as one or two sufficiently stabilized mutants of the GPCR have been identified, these can be used as a basis for the design, construction and screening of potential fusion constructs for crystallization trials in LCP.

Screening of fusion protein constructs for crystallization in LCP ● Timing 3–4 weeks

▲ CRITICAL We adapted the CPM-based high-throughput screening methodology to allow the assessment of (i) suitable fusion proteins for a given receptor and (ii) optimal fusion protein insertion positions, especially as replacement of intracellular loops. These steps were optimized for screening of suitable fusion proteins and insertion positions thereof to replace intracellular loops (ICLs, most often ICL3) of GPCRs.

84 Design a panel of chimeric protein candidates in silico by using a suitable set of fusion proteins, together with predicted secondary structure boundaries of the receptor of interest. As a starting point, three different fusion partners, such as T4L, thermostabilized apocytochrome b_{562} (with mutations M7W, H102I and R106L) and the catalytic domain of PGS can be chosen, as their N- and C-termini have appropriate locations. For each selected fusion protein, three N- and three C-terminal fusion positions should be initially considered to limit the search space.
85 Using the described SLIC approach (Steps 13–17), generate all necessary chimeric receptor constructs.
86 Perform transient transfection, expression, purification and apparent T_m determination as initially established for the GPCR.
87 Analyze the measured data with regard to maximum signal amplitude ΔY (estimation of expression and purification yield) and apparent T_m to determine the influence of each fusion protein as a function of the chosen fusion positions.
88 If needed, design, clone, purify and determine apparent T_m of a second generation of possible crystallization construct candidates. Exclude those fusion proteins and positions that displayed a decrease in maximum raw signal and/or thermostability. The second generation of constructs can be designed by either including a different set of fusion partners (if during the first round of screening no optimal candidate could be identified) or, for those displaying comparable or increased expression and thermostability levels, a focused screen for optimal fusion insertion positions to generate a more diverse panel of potential crystallization candidates.
89 Progress the best-performing chimeric constructs to large-scale expression and purification for initial crystallization trials in LCP.

Troubleshooting

Troubleshooting advice can be found in Table 1.

Table 1 | Troubleshooting table

Step	Problem	Possible cause	Solution
18, 37	Many colonies after SLIC, but only empty vector after sequencing	Vector was not properly linearized	Consider longer restriction digest times and an additional purification by agarose gel electrophoresis to separate fully digested vector from uncut plasmid
25	Low PCR product yield	PCR has not worked	Optimize PCR conditions, e.g., including a lower annealing temperature for the first five amplification rounds
	PCR produces many side products	Primer is not sufficiently specific	Increase length of the primer-target annealing sequence (T_m > 52 °C)

Table continued

Table 1 (continued)

Step	Problem	Possible cause	Solution
35	No colonies after SLIC	*E. coli* cells have not been efficiently transformed	Ensure the added SLIC reaction mixture does not exceed 10% of the total incubation volume
43, 44, 77	Low signal	Poor receptor expression levels. Protein expression is toxic to host cells	Optimize expression parameters. Test shorter expression times, e.g., harvesting of cells after 24 or 48 h after transfection. If receptor overexpression is toxic to the cells, also test expression without addition of Na-butyrate
49, 77	Low signal	Inefficient solubilization of membranes due to inefficient cell lysis	Increase mechanical force, e.g., by stronger vortexing of the cells during cell lysis (Step 49)
71–74, 76	Large deviation between measurements	Deviating incubation time of eluted protein with CPM dye prior to start of T_m determination measurement (Step 75)	Establish a routine with reproducible duration for the preparation of the 96-well qPCR microplate (Steps 71–74). Minimize waiting time prior to starting the measurement (Step 75)
76	Melting curve not sigmoidal, linear slope	Protein aggregation; protein is unstable in the deployed detergent	Add additional washing step to exchange detergent for a milder one. Keep in mind to test the new detergent for possible contribution of fluorescent signal during the CPM assay
		Protein aggregation; protein is not stable in any detergent	Prior engineering of construct necessary, e.g., through introduction of previously described stabilizing mutations
	Uninterpretable melting curve	Ligand (e.g., peptide) is interacting with dye	Test lower ligand concentration. If unsuccessful, use a different ligand
		Excitation and emission spectra of ligand and CPM overlay	Record ligand-only control. Subtract ligand control curve from receptor melting curves. Alternatively, use a different ligand
77	Low signal	Poor expression, despite optimized expression conditions	Prior optimization of screening construct necessary, e.g., truncation of termini and/or introductions of previously described mutations that increase expression levels
89	Construct yields no crystals	Unfavorable protein geometry for crystal packing	Generate and evaluate more chimeric constructs with T_m > 60 °C

Timing

Steps 1–6, design of vector primer pairs: 1 h
Steps 7–12, design of SLIC mutagenesis primer pairs: 1 d
Steps 13–17, design of fusion protein assembly primer pairs: 1 d
Steps 18–41, generation of Ala/Leu scanning mutants: 2–3 weeks
Steps 42–47, transient transfection of mammalian cells with GPCR constructs: 2–3 d
Steps 69–77, determination of the apparent T_m of purified GPCR constructs: 1.5 h
Steps 78–83, combining thermostabilizing mutations to obtain optimally stabilized GPCR mutants: 6–8 weeks
Steps 84–89, screening of fusion protein constructs for crystallization in LCP: 3–4 weeks

Anticipated results

Thermostabilization of OTR in an antagonist-bound conformation

Due to its intrinsically low expression levels and insufficient stability, the OTR had remained inaccessible to structural studies for a long time. To address both of these challenges, an engineering strategy similar to the NK_1R was applied, consisting of a combination of directed evolution and CPM-based thermostabilization.

OTR variants with improved expression levels were selected with two rounds of directed evolution for high expression in yeast[17,88]. However, based on our experience gained from our work with NK_1R (see above), not the most enriched or best functionally expressing OTR variant was selected as a basis for further stabilization, but the most stable. For this purpose, the thermostability of the most enriched yeast-evolved OTR variants was assessed by determining the T_m using our microscale CPM platform (Fig. 6a). For the most stable OTR mutant (OTR-y02), a melting temperature of already 58 °C was determined. We reasoned that introduction of one or two further stabilizing mutations

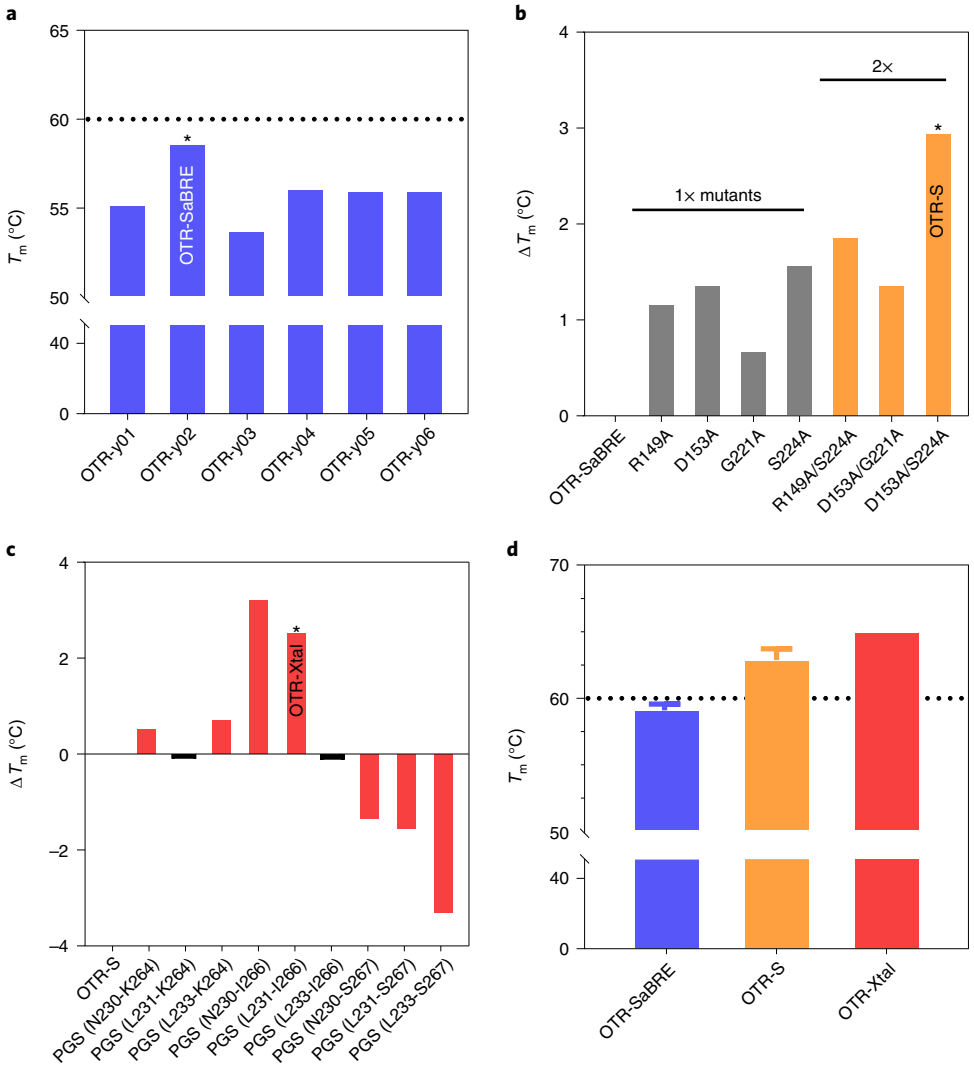

Fig. 6 | Screening and engineering of a successful crystallization construct of the human OTR. a, Apparent T_m of the most enriched OTR variants after selection for high expression in yeast (OTR-y01 to OTR-y06). The most stable clone that was selected as the basis for the creation of a crystallization construct was termed OTR-SaBRE (OTR-y02, marked with an asterisk). **b**, ΔT_m derived from the apparent CPM melting temperature of the most stabilizing single (gray) and double mutants (orange), identified from a limited Ala scan on OTR-SaBRE. The most stable double mutant was termed OTR-S (marked with an asterisk). **c**, ΔT_m derived from the apparent CPM melting temperature of selected PGS insertions replacing the indicated amino acid stretch of OTR-S. The fusion construct used to determine the crystal structure of OTR was termed OTR-Xtal (marked with an asterisk). **d**, Overview of apparent T_m of key OTR constructs. Data shown as average of six, eight and one independent expressions for OTR-SaBRE, OTR-S and OTR-Xtal, respectively, with standard deviations indicated by error bars. Data and colors correspond to panels **a**, **b** and **c**.

should suffice to cross the aimed 60 °C threshold for CPM-T_m. Thus, to accelerate the tailored thermostabilization and save on resources, a limited Ala scan was designed for the OTR.

To select the mutations to be included in the limited Ala scan, the four most beneficial mutations identified in the stabilization of the NK_1R were grafted to the OTR, and all amino acids from −6 to +6 of the respective position were included in the scan. In total, 33 positions at the intracellular ends of transmembrane helices II, IV and VI as well as 11 positions around C219$^{5.57}$ in the middle of helix V were chosen to be tested for their contribution to receptor thermostability. All 44 single-point mutations were cloned, expressed and purified, and their thermostability was determined by recording CPM melting curves according to the provided protocol. Out of the 44 screened single mutants (termed 1x), we identified four mutations with a clearly stabilizing contribution to the apparent T_m. In a next step, double mutants (termed 2x) were created by combining single mutations

from opposing helixes[74] and their thermostability was determined (Fig. 6b). The most stable double mutant (OTR-S) displayed an increased thermostability of 3 °C, compared with OTR-y02. Thus, by testing only 48 mutations and introducing two additional mutations, OTR-S with a CPM-T_m of >60 °C could be generated.

In a final step, we employed CPM-based screening to identify suitable OTR fusion protein insertions to allow efficient crystal contact formation. Guided by the successful structure determination of both the NK_1R[30] and the PTH1R[32] with PGS fusions, the screening space was reduced to OTR–PGS fusions. We generated several OTR chimeras with PGS, replacing ICL3 at varying insertion positions in helices V and VI of the receptor. Among the cloned and tested OTR–PGS fusion constructs, two constructs were identified that displayed a T_m increase of at least 2.5 °C compared with OTR-S (Fig. 6c). Both constructs were expressed in *Sf*9 insect cells, purified on a large scale, reconstituted and readily crystallized within the LCP. Of note, the second most stable construct (OTR-Xtal, Fig. 6c) finally yielded the best diffracting crystals enabling the structure determination of the OTR[31]. Due to the limited screen performed for the OTR, the overall timeline from ordering primers to obtaining initial crystals in LCP could be expedited to ~4 months, including the generation of baculovirus and large-scale purification from expression in *Sf*9 cells.

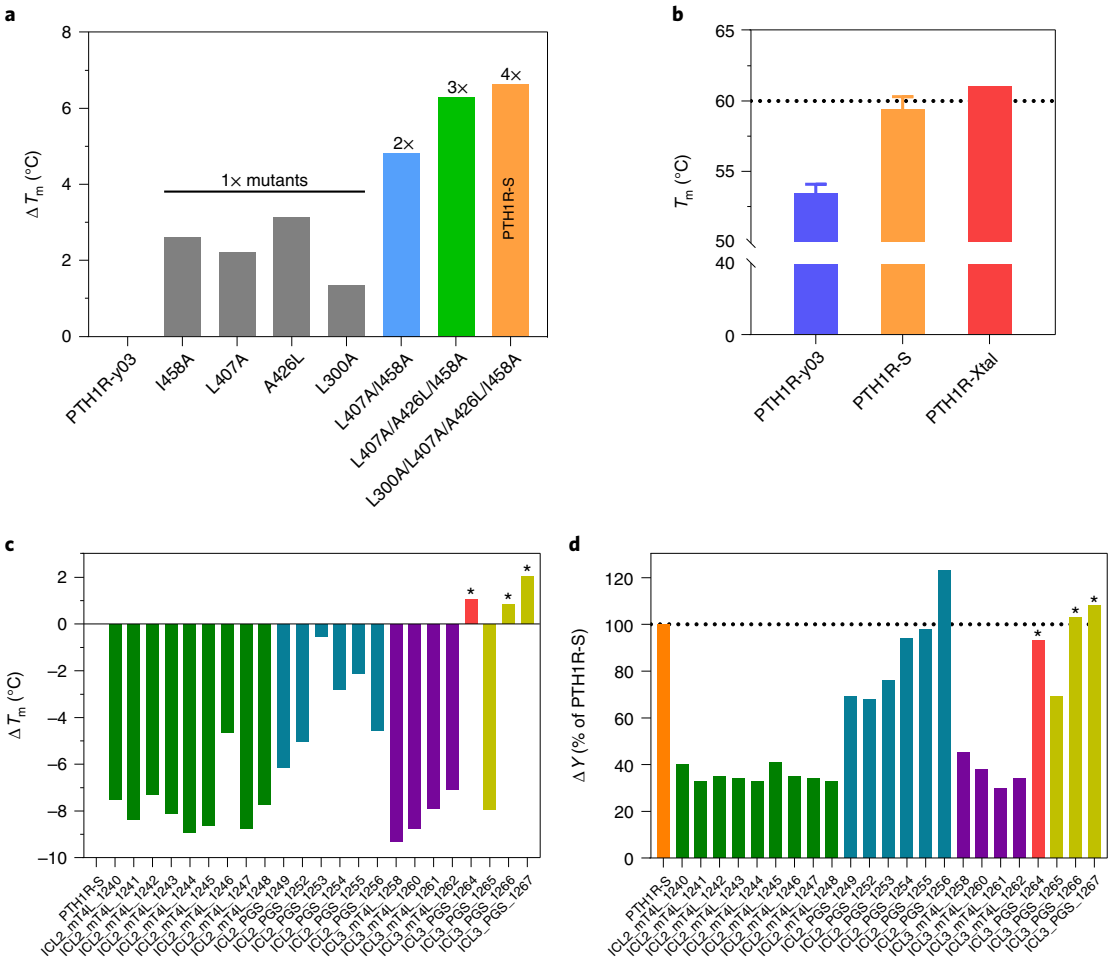

Fig. 7 | CPM-based thermostabilization of PTH1R in an agonist-bound conformation and screening of fusion proteins and their insertion positions. **a**, ΔT_m as determined from the apparent CPM melting temperature of the four single-point mutants (gray bars) and the double (blue bar), triple (green bar) and the quadruple mutant PTH1R-S (orange bar), as compared with the initial variant PTH1R-y03. **b**, T_m as determined from the apparent CPM melting temperature of PTH1R-y03, PTH1R-S and the crystallized PTH1R-S construct containing a PGS fusion in ICL3 (PTH1R-Xtal). Data shown as average of eight, three and one independent expressions for PTH1R-y03, PTH1R-S and PTH1R-Xtal, respectively, with standard deviations indicated by error bars. **c**, ΔT_m of tested chimeric fusion constructs of mT4L and PGS in ICL2 and ICL3 of the receptor compared with the thermostabilized, nonfused mutant PTH1R-S. Colours indicate the type of fusion protein and/or the loop replaced. **d**, Differences in expression and purification yield of the same fusion constructs, expressed as ΔY (Fig. 2c). The ΔY value of each construct is compared with that of PTH1R-S (100%, dashed line). Fusion constructs marked with an asterisk, showing both favorable ΔT_m and ΔY, were selected for large-scale expression in *Sf*9 insect cells and subsequent crystallization trials in LCP. The crystallized construct ICL3_PGS_1264 (PTH1R-Xtal) is highlighted in red.

Thermostabilization of PTH1R in an agonist-bound conformation

The thermostabilization protocol established with NK_1R was also used to successfully tailor the class B GPCR PTH1R in a peptide agonist-bound conformation for crystallization in LCP. Taking the well-expressing receptor mutant PTH1R-y03 obtained from directed evolution in yeast as a basis, 169 single-point mutants to Ala (or Leu if the position already was an Ala) of the transmembrane domain of PTH1R-y03 (residues 178–490) were individually purified and screened for increased receptor thermostability as indicated by their apparent CPM melting temperature.

In the case of PTH1R, identification and introduction of the four combined mutations L300A, L407A, A426L and I458A to PTH1R-y03 yielded a thermostabilized quadruple mutant (PTH1R-S). With a CPM-derived T_m of 60.0 °C, it was 6.6 °C more stable in the CPM assay than the starting variant PTH1R-y03 (T_m of 53.4 °C) (Fig. 7a,b). Fusion construct screening of PTH1R-S with mT4L and PGS, introduced at different insertion positions in ICL 2 and 3 of the receptor, led to the identification of three potential crystallization constructs with enhanced thermostability and acceptable expression and purification yield (Fig. 7c,d).

Prior to transfer to *Sf*9 insect cells, the TMD of PTH1R (ICL3_PGS_1264 (PTH1R-Xtal)) with a CPM-derived T_m of 61.0 °C (Fig. 7b) was genetically re-joined with the extracellular domain of the receptor. After large-scale expression and purification in the presence of a peptide agonist, this construct readily yielded crystals that allowed for the collection of high-resolution diffraction data[32]. For PTH1R, the total process from ordering primers to obtaining initial crystallization hits in LCP took ~10 months, including the generation of baculovirus and large-scale purification from *Sf*9 insect cells.

Reporting Summary

Further information on research design is available in the Nature Research Reporting Summary linked to this article.

Data availability

All data needed to evaluate the conclusions on the paper are present in the paper. The datasets generated and analyzed here are available from the authors upon request.

References

1. Hauser, A. S., Attwood, M. M., Rask-Andersen, M., Schiöth, H. B. & Gloriam, D. E. Trends in GPCR drug discovery: new agents, targets and indications. *Nat. Rev. Drug Discov.* **16**, 829–842 (2017).
2. Katritch, V., Cherezov, V. & Stevens, R. C. Structure–function of the G protein–coupled receptor superfamily. *Annu. Rev. Pharmacol. Toxicol.* **53**, 531–556 (2013).
3. Tesmer, J. J. G. Hitchhiking on the heptahelical highway: structure and function of 7TM receptor complexes. *Nat. Rev. Mol. Cell Biol.* **17**, 439–450 (2016).
4. Xiang, J. et al. Successful strategies to determine high-resolution structures of GPCRs. *Trends Pharmacol. Sci.* **37**, 1055–1069 (2016).
5. Erlandson, S. C., McMahon, C. & Kruse, A. C. Structural basis for G protein–coupled receptor signaling. *Annu. Rev. Biophys.* **47**, 1–18 (2018).
6. Cao, C., Zhang, H., Yang, Z. & Wu, B. Peptide recognition, signaling and modulation of class B G protein-coupled receptors. *Curr. Opin. Chem. Biol.* **51**, 53–60 (2018).
7. Thal, D. M., Glukhova, A., Sexton, P. M. & Christopoulos, A. Structural insights into G-protein-coupled receptor allostery. *Nature* **559**, 45–53 (2018).
8. Serrano-Vega, M. J., Magnani, F., Shibata, Y. & Tate, C. G. Conformational thermostabilization of the β1-adrenergic receptor in a detergent-resistant form. *Proc. Natl Acad. Aci. USA* **105**, 877–882 (2008).
9. Maeda, S. & Schertler, G. F. X. Production of GPCR and GPCR complexes for structure determination. *Curr. Opin. Struc. Biol.* **23**, 381–392 (2013).
10. Rosenbaum, D. M., Rasmussen, S. G. F. & Kobilka, B. K. The structure and function of G-protein-coupled receptors. *Nature* **459**, 356–363 (2009).
11. Kobilka, B. K. Amino and carboxyl terminal modifications to facilitate the production and purification of a G protein-coupled receptor. *Anal. Biochem.* **231**, 269–271 (1995).
12. Cherezov, V. et al. High-resolution crystal structure of an engineered human β2-adrenergic G protein-coupled receptor. *Science* **318**, 1258–1265 (2007).
13. Chun, E. et al. Fusion partner toolchest for the stabilization and crystallization of G protein-coupled receptors. *Structure* **20**, 967–976 (2012).
14. Sarkar, C. A. et al. Directed evolution of a G protein-coupled receptor for expression, stability, and binding selectivity. *Proc.Natl Acad. Aci. USA* **105**, 14808–14813 (2008).
15. Schlinkmann, K. M. et al. Maximizing detergent stability and functional expression of a GPCR by exhaustive recombination and evolution. *J. Mol. Biol.* **422**, 414–428 (2012).

16. Scott, D. J. & Plückthun, A. Direct molecular evolution of detergent-stable G protein-coupled receptors using polymer encapsulated cells. *J. Mol. Biol.* **425**, 662–677 (2013).
17. Schütz, M. et al. Directed evolution of G protein-coupled receptors in yeast for higher functional production in eukaryotic expression hosts. *Sci. Rep.* **6**, 21508 (2016).
18. Magnani, F., Shibata, Y., Serrano-Vega, M. J. & Tate, C. G. Co-evolving stability and conformational homogeneity of the human adenosine A2A receptor. *Proc. Natl Acad. Sci. USA* **105**, 10744–10749 (2008).
19. Tate, C. G. A crystal clear solution for determining G-protein-coupled receptor structures. *Trends Biochem. Sci.* **37**, 343–352 (2012).
20. Zhang, X., Stevens, R. C. & Xu, F. The importance of ligands for G protein-coupled receptor stability. *Trends Biochem. Sci.* **40**, 79–87 (2015).
21. Miller, R. L. et al. The importance of ligand-receptor conformational pairs in stabilization: spotlight on the N/OFQ G protein-coupled receptor. *Structure* **23**, 2291–2299 (2015).
22. Glukhova, A. et al. Structure of the adenosine A1 receptor reveals the basis for subtype selectivity. *Cell* **168**, 867–877.e13 (2017).
23. Hua, T. et al. Crystal structure of the human cannabinoid receptor CB1. *Cell* **167**, 750–762.e14 (2016).
24. Ma, Y. et al. Structural basis for apelin control of the human apelin receptor. *Structure* **25**, 858–866.e4 (2017).
25. Cherezov, V. & Caffrey, M. Nano-volume plates with excellent optical properties for fast, inexpensive crystallization screening of membrane proteins. *J. Appl. Crystallogr.* **36**, 1372–1377 (2003).
26. Cherezov, V. Lipidic cubic phase technologies for membrane protein structural studies. *Curr. Opin. Struc. Biol.* **21**, 559–566 (2011).
27. Cherezov, V., Peddi, A., Muthusubramaniam, L., Zheng, Y. F. & Caffrey, M. A robotic system for crystallizing membrane and soluble proteins in lipidic mesophases. *Acta Crystallogr. D. Biol. Crystallogr.* **60**, 1795–1807 (2004).
28. Magnani, F. et al. A mutagenesis and screening strategy to generate optimally thermostabilized membrane proteins for structural studies. *Nat. Protoc.* **11**, 1554–1571 (2016).
29. Waltenspühl, Y., Ehrenmann, J., Klenk, C. & Plückthun, A. Engineering of challenging G protein-coupled receptors for structure determination and biophysical studies. *Molecules* **26**, 1465 (2021).
30. Schöppe, J. et al. Crystal structures of the human neurokinin 1 receptor in complex with clinically used antagonists. *Nat. Commun.* **10**, 17 (2019).
31. Waltenspühl, Y., Schöppe, J., Ehrenmann, J., Kummer, L. & Plückthun, A. Crystal structure of the human oxytocin receptor. *Sci. Adv.* **6**, eabb5419 (2020).
32. Ehrenmann, J. et al. High-resolution crystal structure of parathyroid hormone 1 receptor in complex with a peptide agonist. *Nat. Struct. Mol. Biol.* **25**, 1086–1092 (2018).
33. Alexandrov, A. I., Mileni, M., Chien, E. Y., Hanson, M. A. & Stevens, R. C. Microscale fluorescent thermal stability assay for membrane proteins. *Structure* **16**, 351–359 (2008).
34. Ayers, F. C., Warner, G. L., Smith, K. L. & Lawrence, D. A. Fluorometric quantitation of cellular and nonprotein thiols. *Anal. Biochem.* **154**, 186–193 (1986).
35. Wang, Z., Ye, C., Zhang, X. & Wei, Y. Cysteine residue is not essential for CPM protein thermal-stability assay. *Anal. Bioanal. Chem.* **407**, 3683–3691 (2015).
36. Cherezov, V., Liu, J., Griffith, M., Hanson, M. A. & Stevens, R. C. LCP-FRAP assay for pre-screening membrane proteins for in meso crystallization. *Cryst. Growth Des.* **8**, 4307–4315 (2008).
37. Chien, E. Y. T. et al. Structure of the human dopamine D3 receptor in complex with a D2/D3 selective antagonist. *Science* **330**, 1091–1095 (2010).
38. Wu, B. et al. Structures of the CXCR4 chemokine GPCR with small-molecule and cyclic peptide antagonists. *Science* **330**, 1066–1071 (2010).
39. Thompson, A. A. et al. Structure of the nociceptin/orphanin FQ receptor in complex with a peptide mimetic. *Nature* **485**, 395–399 (2012).
40. Manglik, A. et al. Crystal structure of the μ-opioid receptor bound to a morphinan antagonist. *Nature* **485**, 321–326 (2012).
41. Wu, H. et al. Structure of the human κ-opioid receptor in complex with JDTic. *Nature* **485**, 327–332 (2012).
42. Liu, W. et al. Structural basis for allosteric regulation of GPCRs by sodium ions. *Science* **337**, 232–236 (2012).
43. Wang, C. et al. Structure of the human smoothened receptor bound to an antitumour agent. *Nature* **497**, 338–343 (2013).
44. Wacker, D. et al. Structural features for functional selectivity at serotonin receptors. *Science* **340**, 615–619 (2013).
45. Wang, C. et al. Structural basis for molecular recognition at serotonin receptors. *Science* **340**, 610–614 (2013).
46. Tan, Q. et al. Structure of the CCR5 chemokine receptor–HIV entry inhibitor maraviroc complex. *Science* **341**, 1387–1390 (2013).
47. Wu, H. et al. Structure of a class C GPCR metabotropic glutamate receptor 1 bound to an allosteric modulator. *Science* **344**, 58–64 (2014).
48. Zhang, J. et al. Agonist-bound structure of the human P2Y12 receptor. *Nature* **509**, 119–122 (2014).
49. Chrencik, J. E. et al. Crystal structure of antagonist bound human lysophosphatidic acid receptor 1. *Cell* **161**, 1633–1643 (2015).
50. Zheng, Y. et al. Structure of CC chemokine receptor 2 with orthosteric and allosteric antagonists. *Nature* **540**, 458–461 (2016).

51. Song, G. et al. Human GLP-1 receptor transmembrane domain structure in complex with allosteric modulators. *Nature* **546**, 312–315 (2017).
52. Wang, S. et al. Structure of the D2 dopamine receptor bound to the atypical antipsychotic drug risperidone. *Nature* **555**, 269–273 (2018).
53. Peng, Y. et al. 5-HT2C receptor structures reveal the structural basis of GPCR polypharmacology. *Cell* **172**, 719–730.e14 (2018).
54. Cao, C. et al. Structural basis for signal recognition and transduction by platelet-activating-factor receptor. *Nat. Struct. Mol. Biol.* **25**, 488–495 (2018).
55. Claff, T. et al. Elucidating the active δ-opioid receptor crystal structure with peptide and small-molecule agonists. *Sci. Adv.* **5**, eaax9115 (2019).
56. Gusach, A. et al. Structural basis of ligand selectivity and disease mutations in cysteinyl leukotriene receptors. *Nat. Commun.* **10**, 5573 (2019).
57. Johansson, L. C. et al. XFEL structures of the human MT2 melatonin receptor reveal the basis of subtype selectivity. *Nature* **569**, 289–292 (2019).
58. Luginina, A. et al. Structure-based mechanism of cysteinyl leukotriene receptor inhibition by antiasthmatic drugs. *Sci. Adv.* **5**, eaax2518 (2019).
59. Stauch, B. et al. Structural basis of ligand recognition at the human MT1 melatonin receptor. *Nature* **569**, 284–288 (2019).
60. Toyoda, Y. et al. Ligand binding to human prostaglandin E receptor EP4 at the lipid–bilayer interface. *Nat. Chem. Biol.* **15**, 18–26 (2019).
61. White, K. L. et al. Structural connection between activation microswitch and allosteric sodium site in GPCR signaling. *Structure* **26**, 259–269.e5 (2018).
62. Yu, J. et al. Determination of the melanocortin-4 receptor structure identifies Ca2+ as a cofactor for ligand binding. *Science* **368**, 428–433 (2020).
63. Xu, F., Liu, W., Hanson, M. A., Stevens, R. C. & Cherezov, V. Development of an automated high throughput LCP-FRAP assay to guide membrane protein crystallization in lipid mesophases. *Cryst. Growth Des.* **11**, 1193–1201 (2011).
64. Li, M. Z. & Elledge, S. J. Harnessing homologous recombination in vitro to generate recombinant DNA via SLIC. *Nat. Methods* **4**, 251–256 (2007).
65. Kuzminov, A. Recombinational repair of DNA damage in *Escherichia coli* and bacteriophage λ. *Microbiol. Mol. Biol. Rev.* **63**, 751–813 (1999).
66. Smith, H. O. & Wilcox, K. W. A restriction enzyme from *Hemophilus influenzae*. I. Purification and general properties. *J. Mol. Biol.* **51**, 379–391 (1970).
67. Gay, P., Le Coq, D., Steinmetz, M., Berkelman, T. & Kado, C. I. Positive selection procedure for entrapment of insertion sequence elements in Gram-negative bacteria. *J. Bacteriol.* **164**, 918–921 (1985).
68. Ghosh, E., Kumari, P., Jaiman, D. & Shukla, A. K. Methodological advances: the unsung heroes of the GPCR structural revolution. *Nat. Rev. Mol. Cell Biol.* **16**, 69–81 (2015).
69. Safarik, I. & Safarikova, M. Magnetic techniques for the isolation and purification of proteins and peptides. *BioMagn. Res. Technol.* **2**, 7 (2004).
70. Brizzard, B. L., Chubet, R. G. & Vizard, D. L. Immunoaffinity purification of FLAG epitope-tagged bacterial alkaline phosphatase using a novel monoclonal antibody and peptide elution. *BioTechniques* **16**, 730–735 (1994).
71. Morrison, K. L. & Weiss, G. A. Combinatorial alanine-scanning. *Curr. Opin. Chem. Biol.* **5**, 302–307 (2001).
72. Faham, S. et al. Side-chain contributions to membrane protein structure and stability. *J. Mol. Biol.* **335**, 297–305 (2004).
73. Yin, J., Mobarec, J. C., Kolb, P. & Rosenbaum, D. M. Crystal structure of the human OX2 orexin receptor bound to the insomnia drug suvorexant. *Nature* **519**, 247–250 (2015).
74. Lebon, G., Bennett, K., Jazayeri, A. & Tate, C. G. Thermostabilisation of an agonist-bound conformation of the human adenosine A2A receptor. *J. Mol. Biol.* **409**, 298–310 (2011).
75. Mirzadegan, T., Benkö, G., Filipek, S. & Palczewski, K. Sequence analyses of G-protein-coupled receptors: similarities to rhodopsin. *Biochemistry* **42**, 2759–2767 (2003).
76. West, G. M. et al. Ligand-dependent perturbation of the conformational ensemble for the GPCR β2 adrenergic receptor revealed by HDX. *Structure* **19**, 1424–1432 (2011).
77. Horcajada, C., Guinovart, J. J., Fita, I. & Ferrer, J. C. Crystal structure of an archaeal glycogen synthase: Insights into oligomerization and substrate binding of eukaryotic glycogen synthases. *J. Biol. Chem.* **281**, 2923–2931 (2006).
78. Thorsen, T. S., Matt, R., Weis, W. I. & Kobilka, B. K. Modified T4 lysozyme fusion proteins facilitate G protein-coupled receptor crystallogenesis. *Structure* **22**, 1657–1664 (2014).
79. Kawate, T. & Gouaux, E. Fluorescence-detection size-exclusion chromatography for precrystallization screening of integral membrane proteins. *Structure* **14**, 673–681 (2006).
80. Shiroishi, M. et al. Platform for the rapid construction and evaluation of GPCRs for crystallography in *Saccharomyces cerevisiae*. *Microb. Cell Fact.* **11**, 78 (2012).
81. Audet, M. et al. Small-scale approach for precrystallization screening in GPCR X-ray crystallography. *Nat. Protoc.* **15**, 144–160 (2020).
82. Klenk, C., Ehrenmann, J., Schütz, M. & Plückthun, A. A generic selection system for improved expression and thermostability of G protein-coupled receptors by directed evolution. *Sci. Rep.* **6**, 21294 (2016).

83. Popov, P. et al. Computational design of thermostabilizing point mutations for G protein-coupled receptors. *eLife* **7**, e34729 (2018).
84. Cherezov, V., Clogston, J., Papiz, M. Z. & Caffrey, M. Room to move: crystallizing membrane proteins in swollen lipidic mesophases. *J. Mol. Biol.* **357**, 1605–1618 (2006).
85. Razinkov, I. et al. A new method for vitrifying samples for cryoEM. *J. Struct. Biol.* **195**, 190–198 (2016).
86. Arnold, S. A. et al. Miniaturizing EM sample preparation: opportunities, challenges, and "visual proteomics". *Proteomics* **18**, 1700176 (2018).
87. Drew, D., Lerch, M., Kunji, E., Slotboom, D.-J. & de Gier, J.-W. Optimization of membrane protein overexpression and purification using GFP fusions. *Nat. Methods* **3**, 303–313 (2006).
88. Waltenspühl, Y., Jeliazkov, J. R., Kummer, L. & Plückthun, A. Directed evolution for high functional production and stability of a challenging G protein-coupled receptor. *Sci. Rep.* **11**, 8630 (2021).

Acknowledgements

We thank G. Meier for his help during transient transfection and expression of protein and would furthermore like to thank F. Zosel for critical reading of the manuscript. This work was supported by Schweizerischer Nationalfonds grant 31003A_153143 and 31003A_182334, and KTI grant 18022.1 PFLS-LS, all to A.P.

Author contributions

J.S. conceptualized the project, devised and established the thermostabilization platform including the expression format and microscale purification technique, performed NK_1R mutagenesis and thermostabilization, and designed and characterized NK_1R crystallization constructs. J.E. devised and established the SLIC-based mutagenesis and construct generation platform and performed the PTH1R thermostabilization and crystallization construct screening. Y.W. performed the OTR thermostabilization and crystallization construct screening with help from J.S. The project was supervised by A.P. The manuscript was prepared by J.S., J.E., Y.W. and A.P. All authors contributed to the final editing and approved of the manuscript.

Competing interests

The authors declare no competing interests.

Additional information

Supplementary information The online version contains supplementary material available at https://doi.org/10.1038/s41596-021-00660-9.

Correspondence and requests for materials should be addressed to Andreas Plückthun.

Peer review information *Nature Protocols* thanks Vadim Cherezov, Isabel Moraes and the other, anonymous, reviewer(s) for their contribution to the peer review of this work.

Reprints and permissions information is available at www.nature.com/reprints.

Publisher's note Springer Nature remains neutral with regard to jurisdictional claims in published maps and institutional affiliations.

Received: 14 August 2021; Accepted: 8 November 2021;
Published online: 09 February 2022

Related links

Key references using this protocol

Ehrenmann, J. et al. *Nat. Struct. Mol. Biol.* **25**, 1086–1092 (2018): https://doi.org/10.1038/s41594-018-0151-4
Schöppe, J. et al. *Nat. Commun.* **10**, 17 (2019): https://doi.org/10.1038/s41467-018-07939-8
Waltenspühl, Y. et al. *Sci. Adv.* **6**, eabb5419 (2020): https://doi.org/10.1126/sciadv.abb5419

nature portfolio

Corresponding author(s): Andreas Plückthun

Last updated by author(s): Sep 29, 2021

Reporting Summary

Nature Portfolio wishes to improve the reproducibility of the work that we publish. This form provides structure for consistency and transparency in reporting. For further information on Nature Portfolio policies, see our Editorial Policies and the Editorial Policy Checklist.

Statistics

For all statistical analyses, confirm that the following items are present in the figure legend, table legend, main text, or Methods section.

n/a	Confirmed	
☐	☒	The exact sample size (*n*) for each experimental group/condition, given as a discrete number and unit of measurement
☐	☒	A statement on whether measurements were taken from distinct samples or whether the same sample was measured repeatedly
☒	☐	The statistical test(s) used AND whether they are one- or two-sided *Only common tests should be described solely by name; describe more complex techniques in the Methods section.*
☒	☐	A description of all covariates tested
☒	☐	A description of any assumptions or corrections, such as tests of normality and adjustment for multiple comparisons
☐	☒	A full description of the statistical parameters including central tendency (e.g. means) or other basic estimates (e.g. regression coefficient) AND variation (e.g. standard deviation) or associated estimates of uncertainty (e.g. confidence intervals)
☒	☐	For null hypothesis testing, the test statistic (e.g. *F*, *t*, *r*) with confidence intervals, effect sizes, degrees of freedom and *P* value noted *Give P values as exact values whenever suitable.*
☒	☐	For Bayesian analysis, information on the choice of priors and Markov chain Monte Carlo settings
☒	☐	For hierarchical and complex designs, identification of the appropriate level for tests and full reporting of outcomes
☒	☐	Estimates of effect sizes (e.g. Cohen's *d*, Pearson's *r*), indicating how they were calculated

Our web collection on statistics for biologists contains articles on many of the points above.

Software and code

Policy information about availability of computer code

Data collection	No custom software or code was used.
Data analysis	No custom software or code was used.

For manuscripts utilizing custom algorithms or software that are central to the research but not yet described in published literature, software must be made available to editors and reviewers. We strongly encourage code deposition in a community repository (e.g. GitHub). See the Nature Portfolio guidelines for submitting code & software for further information.

Data

Policy information about availability of data

All manuscripts must include a data availability statement. This statement should provide the following information, where applicable:

- Accession codes, unique identifiers, or web links for publicly available datasets
- A description of any restrictions on data availability
- For clinical datasets or third party data, please ensure that the statement adheres to our policy

The datasets generated and analysed here are available from the authors upon request

Field-specific reporting

Please select the one below that is the best fit for your research. If you are not sure, read the appropriate sections before making your selection.

☒ Life sciences ☐ Behavioural & social sciences ☐ Ecological, evolutionary & environmental sciences

For a reference copy of the document with all sections, see nature.com/documents/nr-reporting-summary-flat.pdf

Life sciences study design

All studies must disclose on these points even when the disclosure is negative.

Sample size	The study was based on expression, purification and melting temperature determination of individual proteins. Stabilizing mutations and combinations thereof were selected from single melting temperature measurements on individually expressed and purified proteins. A reference construct was included in every measurement as a control.
Data exclusions	No data were excluded.
Replication	Single melting temperature measurements were performed on individually expressed and purified proteins. Where applicable (e.g. control constructs) measurements from several independently expressed and purified proteins were averaged.
Randomization	n/a
Blinding	n/a

Reporting for specific materials, systems and methods

We require information from authors about some types of materials, experimental systems and methods used in many studies. Here, indicate whether each material, system or method listed is relevant to your study. If you are not sure if a list item applies to your research, read the appropriate section before selecting a response.

Materials & experimental systems

n/a	Involved in the study
☒	☐ Antibodies
☐	☒ Eukaryotic cell lines
☒	☐ Palaeontology and archaeology
☒	☐ Animals and other organisms
☒	☐ Human research participants
☒	☐ Clinical data
☒	☐ Dual use research of concern

Methods

n/a	Involved in the study
☒	☐ ChIP-seq
☒	☐ Flow cytometry
☒	☐ MRI-based neuroimaging

Eukaryotic cell lines

Policy information about cell lines

Cell line source(s)	Only HEK293T/17 cells were used, obtained from ATCC (number: CRL-11268).
Authentication	No authentication was used, as the experiments depend only on transient transfection of a recombinant protein.
Mycoplasma contamination	Since the cells were freshly obtained from ATCC, no mycoplasma testing was used.
Commonly misidentified lines (See ICLAC register)	n/a